TÉCNICO LISBOA

Methane production from CO_2 over Ni-hydrotalcite derived catalysts

Keerthivarman Veerappanchatram Kaliappan

Thesis to obtain the Master of Science Degree in

Energy Engineering and Management

Supervisors: Prof. Maria Filipa Gomes Ribeiro

Prof. Carlos Manuel Faria de Barros Henriques

Prof. Teresa Grzybek

Examination Committee

Chairperson: Prof. Maria de Fátima Grilo da Costa Montemor

Supervisor: Prof. Maria Filipa Gomes Ribeiro

Member of the committee: Prof. José Manuel Félix Madeira Lopes

October 2016

“It always seems impossible until it’s done”

(Nelson Mandela)

Acknowledgment

First of all, I would like to express my sincere gratitude to my supervisors from *Instituto Superior Técnico*: Prof. Filipa Ribeiro and Prof. Carlos Henriques and to my supervisor from AGH University of Science and Technology, Prof. Teresa Grzybek for their continuous support and motivation throughout the course of my research without whom this thesis wouldn't have seen the light of the day.

I would like to express my humblest thanks to KIC InnoEnergy for their master's scholarship and assistance throughout the course of this degree.

I would also like to thank Carminha and Dominik Wierzbicki who amidst their busy doctoral studies assisted me with the laboratory works and solved my experimental doubts. Special thanks to them, who with their passionate participation and input made the laboratory experiments more fun and interesting.

In addition, I express my thanks to Dr. Auguste and Cátia for sharing their valuable thoughts during the progress of this work. I thank my fellow labmates Raquel, Diogo, Duarte and Paula for their stimulating discussions and support.

Finally, I must express my very profound gratitude to my family for providing me with unfailing support and continuous encouragement throughout study and through the process of researching and writing this thesis. This accomplishment would not have been possible without them.

Abstract

Hydrogenation of carbon dioxide to methane has been reported as one of the most favorable option for the reduction of CO_2 emissions. In the literature, different metal based catalysts have been studied for this reaction being Ni based catalysts the most widely investigated one. The properties of mixed oxides derived from hydrotalcites are interesting for catalytic applications such as CO_2 methanation. In this work, Ni-hydrotalcite derived catalysts (Ni, Mg, Al mixed oxides) with different Ni content and x ratios (x=Al/(Al+Mg+Ni)) were prepared by co-precipitation method, characterized by Fourier Transform-Infrared spectroscopy (FT-IR), Thermogravimetric analysis (TGA), X-Ray diffraction (XRD), Low temperature nitrogen sorption, Hydrogen temperature programmed reduction (H_2-TPR), H_2 and CO_2 Temperature programmed desorption and Scanning Electron Microscopy (SEM). Samples were finally tested to evaluate their catalytic performances in terms of CO_2 conversion and CH_4 selectivity. All samples synthesized in the present work revealed interesting catalytic performances towards CO_2 methanation. Ni content seemed to slightly favor both conversion and selectivity probably due to the enhancement of the Ni species reducibility and x ratio did not have strong influence in the catalytic results. Samples remained stable after 24h test and more active for CO_2 methanation than a commercial catalyst containing similar Ni amount over Al_2O_3.

Keywords: Carbon dioxide, Methanation, hydrotalcite, Ni, Co-precipitation, mixed oxides

Resumo

A conversão de CO_2 a metano é considerada uma das alternativas mais favoráveis para a redução das emissões deste gás de efeito estufa. Na literatura foram utilizados catalisadores baseados em diferentes metais e suportes, sendo que o Ni foi referido como o metal mais promissor. Os óxidos mistos formados a partir da calcinação de hidrotalcitas contendo Ni, Mg e Al têm propriedades interessantes para a sua utilização como catalisadores na metanação do CO_2. Neste trabalho estudaram-se catalisadores derivados de hidrotalcitas preparados por co-precipitação, os quais foram testados na reacção de hidrogenação do CO_2. Os catalisadores preparados contêm diferentes quantidades de Ni e a percentagem de catiões bi e trivalentes, expressa pela razão x= Al/(Al+Mg+Ni) foi igualmente alterada. As amostras foram caracterizadas por FTIR, TGA, XRD, adsorção de N_2, H_2-TPR, H_2-TPD, CO_2-TPD e SEM. Finalmente foram testadas em condições de metanação com o fim de determinar a conversão de CO_2 assim como a selectividade para o CH_4. Todas as amostras apresentaram resultados interessantes nos testes catalíticos sendo que o aumento na quantidade de Ni conduziu a uma melhoria dos resultados. Contudo, as alterações na composição química (x) das hidrotalcitas não levou a mudanças significativas. Concluiu-se ademais que os catalisadores são estáveis em condições de teste catalítico durante pelo menos 24 horas e que, quando comparados com um catalisador comercial com uma quantidade de Ni semelhante e suportado em Al_2O_3, apresentam melhores resultados.

Palavras-chave: Dióxido de carbono, metanação, hidrotalcita, Ni, co-precipitação, óxidos mistos

Index

List of Tables

List of Figures

Abbreviations

GHG: Greenhouse Gas

INDC: Intended Nationally Determined Contribution

CCS: Carbon Capture and Sequestration

RWGS: Reverse Water – Gas Shift

LDH: Layered Double Hydroxide

FT-IR: Fourier Transform Infrared

TGA: Thermogravimetric Analysis

XRD: X – Ray Diffraction

TPR: Temperature Programmed Reduction

TPD: Temperature Programmed Desorption

SEM: Scanning Electron Microscopy

1. Introduction

In recent times, global CO_2 emissions are increasing at an alarming rate and for the first time in the history the carbon dioxide concentration has reached more than 400 ppm in a non-industrial region (measured on August 2015 at Mauna Loa Observatory, Hawaii). The most important reason for CO_2 emission increase is fossil fuel usage in power plants, industries and transportation sector. This increase has caused major environmental problems like global warming, climate change, ocean acidification, to name a few. Hence it is of utmost importance to find ways of reducing carbon dioxide emissions for the betterment and sustenance of life on earth.

There are several strategies advocated for the mitigation of carbon dioxide emissions, the most favorable being the use of carbon dioxide as raw material for the production of chemicals and fuels. At this moment CO_2 is already used for the production of certain chemicals such as urea and its derivatives, organic carbonates, salicylic acid, methanol, etc. However, the production of fuels may significantly contribute to the reduction of carbon dioxide emissions due to the higher consumption rates of the fuels sector. Fuels can be produced through the hydrogenation of CO_2 to oxygenates and/or hydrocarbons (e.g. methanol, dimethyl ether or methane). Carbon dioxide methanation remains advantageous among various CO_2 hydrogenation reactions in terms of thermodynamics and reaction rate. In addition, methane is the main component of natural gas, a fossil fuel widely consumed besides coal and oil, which has a well-established infrastructure for transportation and storage.

Although carbon dioxide methanation reaction is thermodynamically favored, it requires a catalyst to activate the stable CO_2 molecule and reduce it to methane. Mostly catalysts based on metals from group VIIIB (Fe, Ni, Ru, Rh and Pd) have been studied, being Ni the most widely investigated due to their high efficiency in CH_4 production and low cost. Supports such as SiO_2, TiO_2, Al_2O_3, ZrO_2, CeO_2, and Ce – Zr mixed oxides, have been also reported for this reaction. In earlier works, significant levels of CO_2 conversion and CH_4 selectivity in CO_2 methanation reaction were reported using Ni – hydrotalcite derived catalysts.

Thus, in this MSc thesis Ni – hydrotalcite derived catalysts (Ni, Mg, Al mixed oxides) were prepared by co–precipitation method with different Ni content and x ratio (Al/Al+Mg+Ni). All the samples were characterized by ICP analysis, Fourier Transform Infrared (FT-IR) spectroscopy, Thermogravimetric Analysis (TGA), X- ray diffraction (XRD), Low temperature nitrogen sorption, H_2-Temperature Programmed Reduction, H_2 and CO_2 Temperature Programmed Desorption and Scanning Electron Microscopy (SEM). After the characterizations, catalysts were tested under CO_2 methanation conditions and CO_2 conversions and CH_4 selectivity were determined. Results were compared with a commercial Ni/Al_2O_3 catalyst tested under the same conditions. A long term test of 24 hours under reaction conditions was also carried out for one of the prepared catalysts in order to evaluate its stability.

2. Literature Review

2.1. CO_2 as Greenhouse Gas

Human activities have recently led to an increase of Greenhouse Gases (GHG) concentration in the atmosphere, as illustrated by the Figure 1. The amount of three main GHG emissions, carbon dioxide (CO_2), methane (CH_4) and nitrous oxide (N_2O) have been increasing since the pre-industrial times, and this has been assigned as one of the main causes of climate change. Carbon dioxide is present in the atmosphere and is a part of natural carbon cycle of Earth. Human activities, however, have altered the carbon cycle by both - adding more CO_2 to the atmosphere and influencing the ability of the natural sinks, such as forests and ocean, to remove the CO_2 from the atmosphere [1]. Between 1750 and 2011, CO_2 concentration in the atmosphere has increased by 40% from 278ppm to 390.5ppm. In August 2015, for the first time in a non-industrial region (Mauna Loa Observatory, Hawaii) CO_2 concentration attained more than 400ppm.

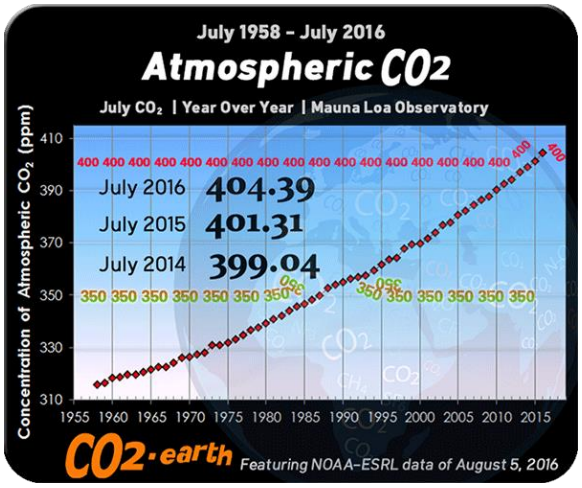

Figure 1: Trends in atmospheric carbon dioxide [2]

This observed increase is mainly due to the fossil fuel combustion, which is one of the main methods of producing energy [3] as shown in the Figure 2.

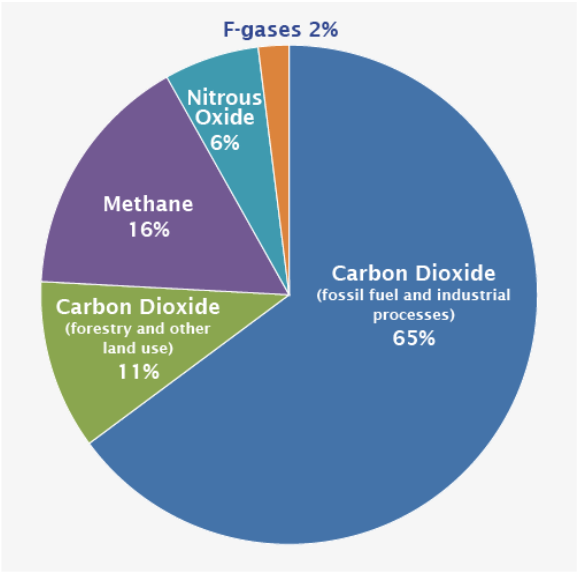

Figure 2: Share of Global GHGs 2010 (F-gases include hydrofluorocarbons (HFCs), perfluorocarbons (PFCs), and sulfur hexafluoride (SF_6)) [4]

Worldwide economic growth and development have led to the increasing demand for energy. Figure 3 compares Total Primary Energy Supply (TPES) between the years 1971 and 2013. As shown in the Figure 3, it increased by an enormous amount of 150%, mainly relying on fossil fuels, which in 2013 accounted for around 82% of the TPES. Thus fossil fuels having the prominent share in TPES, plays a key role in the upward trend of CO_2 emissions [5].

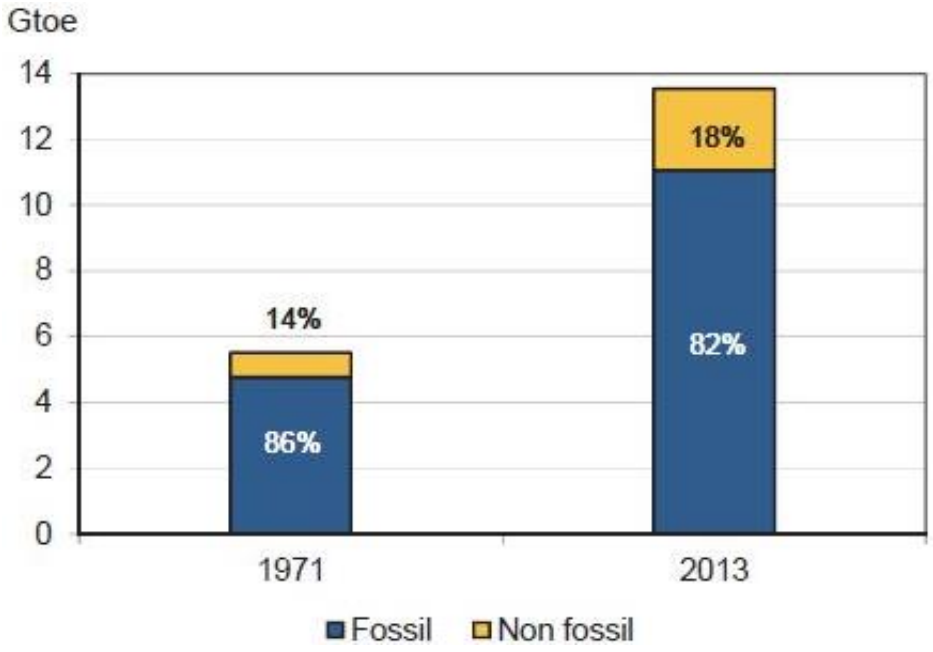

Figure 3: World Primary Energy Supply [6]

In order to reduce the CO_2 emissions and, at the same time, maintain the global economic growth, development of CO_2 abatement technologies is essential which could lead to the reduction of CO_2 impact on climate change.

2.2. CO_2 mitigation approaches

Several countries have submitted the 'Intended Nationally Determined Contributions (INDCs)' prior to the 21st UN Conference of Parties (COP21) held at Paris in December 2015. Intended Nationally Determined Contributions (INDCs) submitted by countries contain commitments relating to the energy sector and, the assessment of the impact of these INDCs and related policy statements on future energy trends is presented as "INDC Scenario". Figure 4 depicts a comparison between the INDCs Scenario and 450 Scenario (450 Scenario – reflects a pathway consistent with around a 50% chance of meeting the 2 °C climate goal), which shows that by 2030 there will be a 9 Gt gap between energy-related emissions in the INDC Scenario and the 450 Scenario [7]. This requires better CO_2 mitigation approaches. Some of the strategies in the reduction of CO_2 emissions are discussed in this section [8].

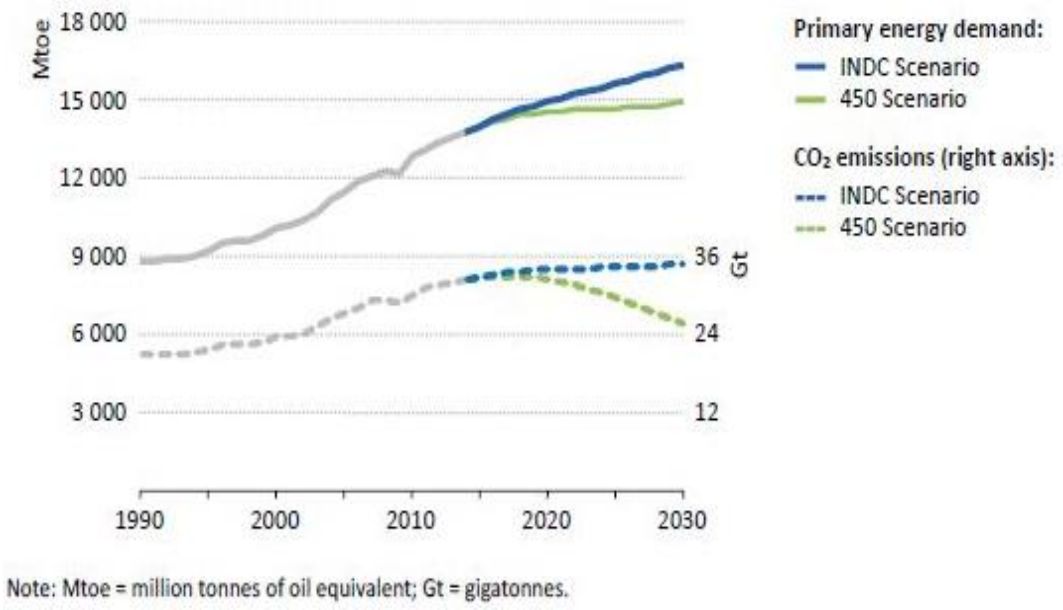

Figure 4: Global primary energy demand and related CO_2 emissions by scenario [7]

2.2.1. Reduction in the amount of CO_2 produced

The primary and the best strategy would be to reduce the amount of CO_2 produced at source which could be done by energy efficiency improvements, development of large-scale renewable energy production plants, switching from fossil fuels to less carbon intensive fuel such as hydrogen [9].

2.2.2. Storage of CO_2 – Carbon Capture and Sequestration (CCS)

Carbon Capture and Sequestration technology proposed for the capture of CO_2 produced in fossil fuel power plants and industries is illustrated in Figure 5. It consists of removal of carbon dioxide from flue gases, its transport through pipes or ships, and storage in depleted oil/gas fields, un-minable coal fields or in deep marine aquifers. As of mid-2013, CCS has not yet been applied on a large scale to bigger commercial fossil-fired power generation facility, however five individual large end-to-end commercial CCS facilities were in operation around the world. Collectively, they have stored more than 30 Mt CO_2 over their lifetimes [10]. The biggest market for CCS is in power generation sector. Since the CCS is an expensive technology, stringent limits on GHG emissions and economic subsidies from the government are required for the large scale commercialization.

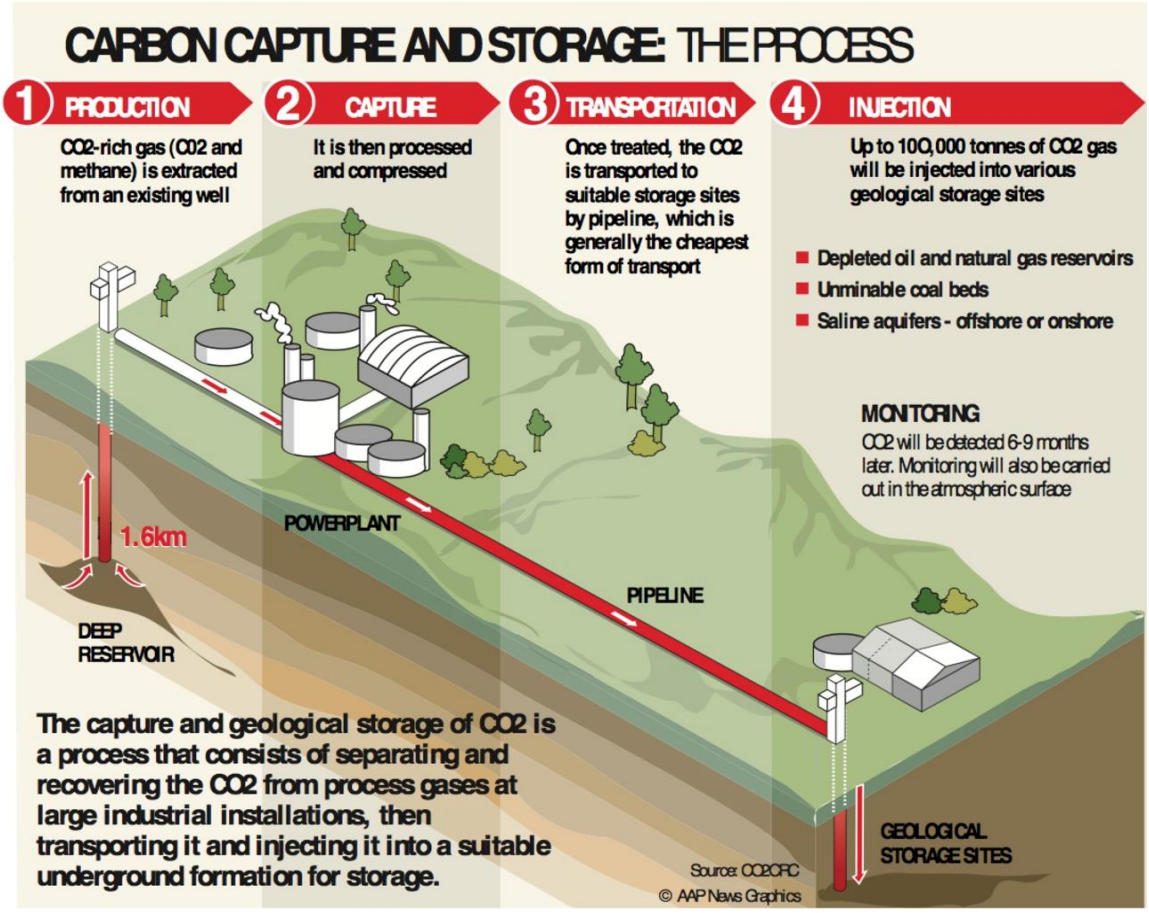

Figure 5: Carbon Capture and Sequestration [11]

2.2.3. Utilization of CO_2

An alternative strategy in reducing CO_2 emissions is to convert CO_2 into valuable chemicals and fuels. The utilization of CO_2 as a substrate to produce chemicals and fuels appears to be an attractive business opportunity, in contrast to considering CO_2 as a waste with considerable costs of disposal [12]. It can be roughly estimated that about 5–10% of the total CO_2 emissions (about 30 Gt worldwide in 2008) could be suited for production of fuels and chemicals, e.g. about one order of magnitude higher than actual use of CO_2 in industry [13].

There are many advantages and opportunities for industries using CO_2 as a carbon source. Some of them are [13]:

- Decrease in costs for CO_2 disposal or emission reduction credits;
- Use as a nontoxic, noncorrosive, and nonflammable reactant, which can be easily stored in the liquid form under mild pressure, leading to safety and environmental benefits in process development;
- Development of innovative processes and products using a feedstock of low or even negative value, and possible gain in market share;
- Improvement of the public image for their contribution in converting a greenhouse gas onto valuable chemicals or fuels;
- Possible CO_2 chemical recycling using renewable resources (solar energy); and

- Production of fuels from CO_2 which integrate within the existing infrastructure and; having a higher energy density and easier transport/storage than competing solutions (hydrogen, in particular).

In general, there are four main approaches to convert CO_2 [14]:

1. To use high-energy starting materials, such as hydrogen, unsaturated compounds, small-membered ring compounds, and organometallics.
2. To choose oxidized low-energy synthetic targets, such as organic carbonates.
3. To shift the equilibrium to the product side by removing a particular compound.
4. To supply physical energy, such as light or electricity.

2.2.3.1. CO_2 as feedstock for chemicals

CO_2 being an economical, renewable and safe carbon source turns out to be an attractive C1 building block of many organic chemicals, materials and carbohydrates [15]. Despite its advantages, CO_2 is not extensively used as a feedstock in current laboratory and industrial processes. Until now, only a few industrial processes, such as synthesis of urea and its derivatives, production of methanol, salicylic acid and polycarbonates (for plastics), have been using CO_2 as the substrate, or as in case of methanol an additional substrate beside the main one (CO). This is primarily due to the thermodynamic stability of CO_2 and thus high energy substances or electro-reductive processes are typically required to transform CO_2 into other chemicals [8].

Lately, in small scales, there is an increasing utilization of carbon dioxide as a fluid in dry-cleaning, refrigerators, air conditioners, fire-extinguishers, separation techniques, water treatment and the food- or agro-chemical industry. Supercritical-CO_2 finds an application as a solvent for reactions, nano-particle or -composite production, and polymer-modification [16].

2.2.3.2. CO_2 for fuel production

The actual use of CO_2 corresponds to a few percentage of potential CO_2 suitable for conversion to chemicals. Therefore, a chemical recycling of CO_2 may significantly contribute to the reduction of its emissions only, when the target products are components for the fuel pool, which worldwide consumption is two order of magnitude higher than that of chemicals. In order to reduce CO_2 emissions significantly and to create high economic value, the main products of CO_2 conversion must be fuels, although some of them (methanol, ethanol, etc.) could be considered in the double role of fuel and chemical. In addition, valorization of carbon dioxide emissions could be one of important parts of the general strategy for reducing CO_2 emissions and push chemical and energy companies towards a more sustainable use of the resources [13].

There are different options to convert carbon dioxide. Hydrogen is a high energy material and can be used for the transformation of carbon dioxide. The main products of carbon dioxide hydrogenation are shown in Figure 6.

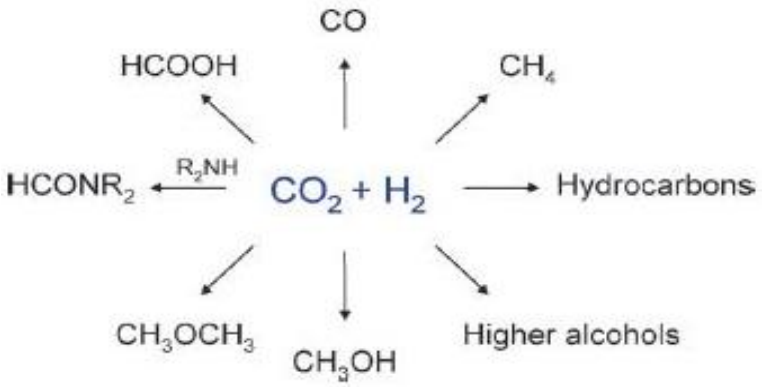

Figure 6: Products of Carbon dioxide hydrogenation [8]

Hydrogenation to oxygenates and/or hydrocarbons is the most intensively investigated area of CO_2 conversion. Methanol synthesis from CO_2 and H_2 has been investigated at the pilot plant stage with promising results. The alternative possibility is the production of DME, a clean-burning fuel that is a potential diesel substitute. Ethanol formation, either directly or via methanol homologation, or the conversion of CO_2 to formic acid, are also potentially interesting routes. Methanol, ethanol, and formic acid may be used as feedstock in fuel cells, providing a route to store energy from CO_2 and then produce electricity [13].

Considering the thermodynamics of the process, the methanation of carbon dioxide remains advantageous among various CO_2 hydrogenation reactions. Furthermore, this reaction is considerably faster than the other reactions producing hydrocarbons. Another beneficial factor of methanation of CO_2 is that methane is the main component of natural gas, a fossil fuel widely consumed besides coal and oil, which has a well-established infrastructure for transportation and storage.

2.3. Methanation of CO_2

Hydrogenation of carbon dioxide to methane, also known as Sabatier reaction, is an important catalytic process. The methanation of carbon dioxide has a wide range of applications. One of interesting possibilities is using this process for the manned colonization of Mars. The research of such application is carried out at NASA [17]. With this process, it may be possible to convert Martian CO_2 to methane and water for fuel and astronaut life support systems. The methanation of CO_2 is thermodynamically favorable (ΔG_{298K}= -130.8 kJ mol^{-1}). However, the reduction of the fully oxidized carbon to methane is an eight-electron process with significant kinetic limitations, which thus requires a catalyst to achieve acceptable rates and selectivities [18]. There are three independent reactions during the methanation process [19]:

$$CO_2 + 4H_2 \rightarrow CH_4 + 2H_2O, \quad \Delta H_{298K} = -164.747\ kJmol^{-1} \text{ ----------}i$$

$$CO_2 + 2H_2 \rightarrow C + 2H_2O, \quad \Delta H_{298K} = -90.147\ kJmol^{-1} \text{ ----------}ii$$

$$CO_2 + H_2 \rightarrow CO + H_2O, \quad \Delta H_{298K} = 41.138\ kJmol^{-1} \text{ ----------}iii$$

2.3.1. Catalysts for CO_2 Methanation

Although carbon dioxide methanation reaction is thermodynamically favored, it requires a catalyst to activate the stable CO_2 molecule and reduce it to methane. The main secondary product of this reaction is carbon monoxide, which can be formed through reverse water gas shift reaction (RWGS) and/or through intermediary reactions. Hence a proper selection of a catalyst is essential for the good selectivity towards CH_4. Methanation of CO_2 has been studied over a wide range of supports and metals. The following table lists the catalysts which have been reported in literature since 2000.

Table 1: The list of studied methanation catalysts, reported in literature from 2000

Catalysts		**Reference**
Metal	**Support**	
Fe	Silica	[20]
Ni, Cu	Activated non –woven carbon materials	[21]
Pd	Mg/SiO_2	[18]
Pd	CeO_2	[22]
Ni	$RHA\text{-}Al_2O_3$	[23]
Ni	ZrO_2	[24]
Ni	MCM-41	[25]
Ru	TiO_2	[26]
Ni	$Ce\text{-}ZrO_2$ mixed oxide	[27]
$LaNiO_3$ perovskite		[28]
Pd-Mg	SiO_2	[18]
Ni	La_2O_3	[29]
Ru	Carbon nanofibers	[30]
Ni/Rh	Al_2O_3	[31]
Ru	CeO_2	[32]
$Ni–Ce_xZr_{1-x}O_2$		[33]
Ni	$ZrO_2\text{-}Al_2O_3$	[34]
Ni-La/SiC		[35]
Ni-CeO2/Al2O3		[36]
Ni	ZrO_2	[37]
Rh	$\gamma\text{-}Al_2O_3$	[38]
$Ni\text{-}Fe\text{-}Al_2O_3$		[39]
Ni-Al mixed oxide		[40]
Co	KIT-6	[41]
Co	Meso- SiO_2	[41]
$Ni\text{-}Fe\text{-}Ru\text{-}Al_2O_3$		[42]
Ni	HNaUSY Zeolite	[43]
Ni	$\gamma\text{-}Al_2O_3$	[44]
Ni, Ru, Rh, Fe, Cu, Ir	MSN	[45]
$Ni/MgO/SiO_2$		[46]

(Continuation Table 1)

Catalysts		Reference
Metal	**Support**	
$Ru/Mn/Ce/Al_2O_3$		[47]
Ni	Al_2O_3	[48]
Ni	$Ce_{0.5}Zr_{0.5}O_2$	[49]
Ru/Pd/Mn/Ni	Al_2O_3	[50]
Ru, Ni	Al_2O_3	[51]
Ni	$MgAl_2O_4$	[52]
Ni-Fe, Co, Cu	ZrO_2	[53]
Ni	CeO_2	[54]
Cu-K	Al_2O_3	[55]
Ru/Mn/Sr	Al_2O_3	[56]
NI/Ru/Rh/Ce/Zr	Al_2O_3	[57]
Ru/Mn/Sr/Ce	Al_2O_3	[58]
$NiAl(O)_x$		[59]
HTNi-CeZr		[60]
Ru	γ-Al_2O_3	[61]
Ni, La	Hydrotalcite	[62]
W	Ni-Mg mixed oxide	[63]

2.3.2. Reaction mechanism

Although the methanation of CO_2 is a comparatively simple reaction, its mechanism appears to be difficult to establish. There are different opinions on the nature of the intermediates and the methane formation process. The reaction mechanisms proposed for CO_2 methanation fall mainly into two categories: conversion of CO_2 to CO prior to methanation and the subsequent reaction following the same mechanism as CO methanation [21] and direct hydrogenation of CO_2 to methane without the formation of CO as the intermediate [64].

It should be additionally mentioned that, even for CO methanation, there is still no consensus on the kinetics and mechanism. It has been proposed that the rate-determining step is either the formation of the CH_xO intermediate and its hydrogenation or the formation of surface carbon in CO dissociation and its interaction with hydrogen [21,65].

One of the main factors which influence the reaction mechanism is the catalyst used. The type of metal, the type of promoters and the selected support influences the reaction mechanism [66].

Recent studies for determining the mechanism of CO_2 methanation reaction were carried out using different supports. One of them was ceria-zirconia support [67]. The result of this study shows that the main mechanism for methanation does not require CO as the reaction intermediate. It is postulated that H_2 dissociates on Ni sites while CO_2 is activated on the ceria-zirconia support to form carbonates which will be hydrogenated into formates and further into methoxy species. This

mechanism involves weak basic sites of the support for the adsorption of CO_2. The proposed reaction mechanism is shown in the Figure 7.

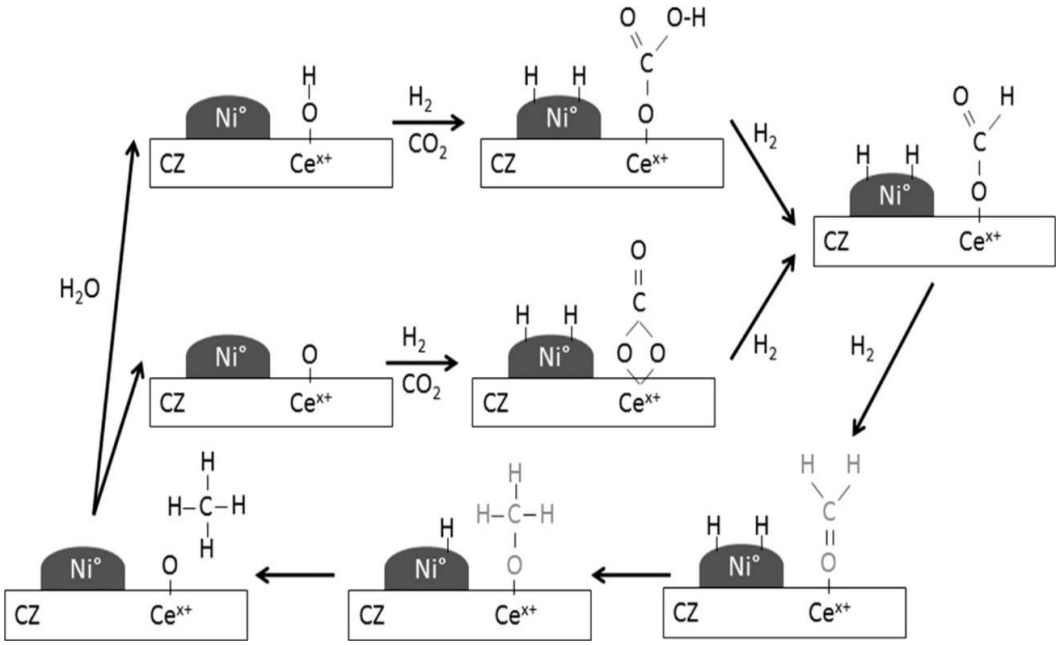

Figure 7: Reaction mechanism proposed on Ni-CZ sol-gel sample for CO_2 Methanation [67]

Another study was carried out using zeolite based catalyst [68]. As illustrated by the Figure 8, this study shows that CO_2 hydrogenation mechanism does not progress through formation of carbonate as an intermediate, but rather passes through the formate dissociation onto Ni^0 particles, leading at low temperatures to the formation of adsorbed CO and, in a minor way, to methane. CO seems to be the intermediate in the CO_2 methanation reaction in this catalytic system. According to Westermann et al [68] the simultaneous measurements of both adsorbed and gaseous species seems to confirm previous conclusions in the literature indicating that the CO dissociation/hydrogenation is the rate-determining step for the CO_2 methanation. The mechanism is explained through Figure 8.

In order to understand the mechanism over hydrotalcite support, Fan et al. analyzed the reaction over $Ni/MgAl_2O_4$ samples prepared by different decomposition methods. According to this study, CO is an intermediate in the CO_2 methanation. It is found that at temperature above 200° C surface carbonyls were produced which was verified by adsorption. Since 200° C is the temperature at which the catalysts starts to show activity in CO_2 methanation, CO appears to be the reaction intermediate. Carbonate species were also found to be adsorbed onto Ni^0 particle or the support. However, it was demonstrated that carbonate species were formed without the presence of H_2 and Ni^0, which indicated that surface carbonates might arise from surface reaction between CO_2 with O_2^- of the support and they appear to be only “spectator” species [52].

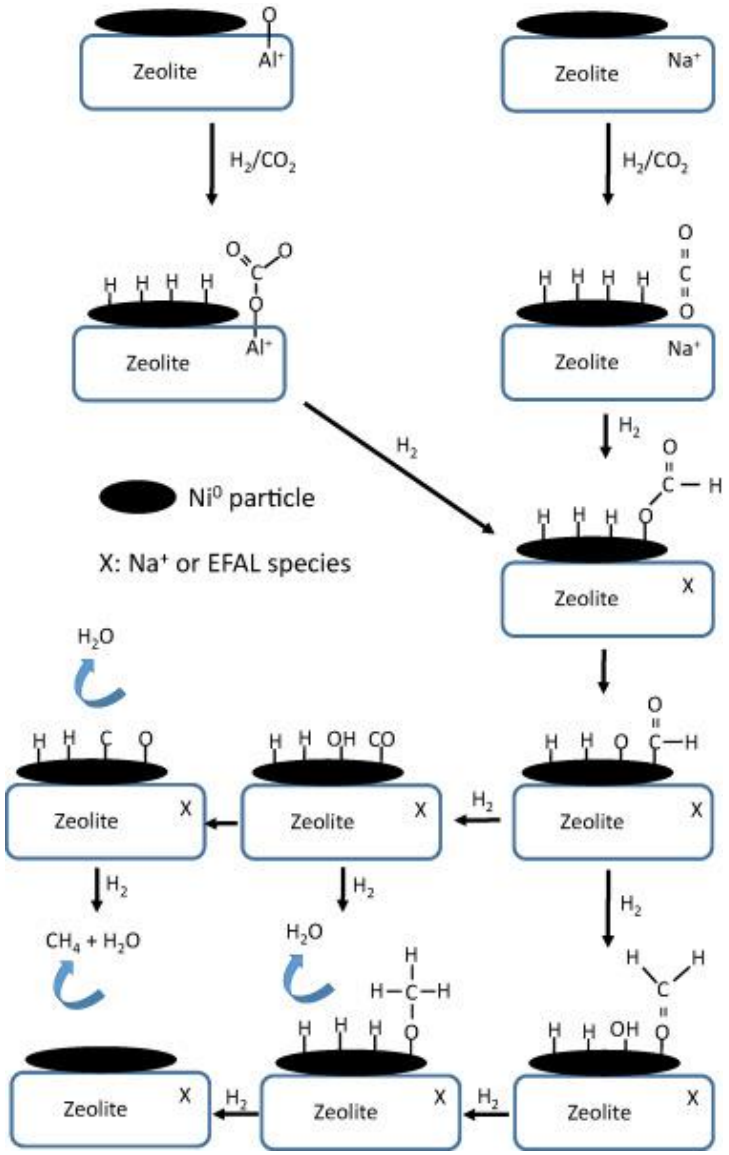

Figure 8: Proposed mechanism for CO2 hydrogenation on NiUSY zeolites [68]

2.4. CO_2 Methanation using Hydrotalcite catalysts

2.4.1. Introduction

Anionic clays based on hydrotalcite type compounds have many practical applications, as presented in the Figure 9, and they can be used as such or after calcination:

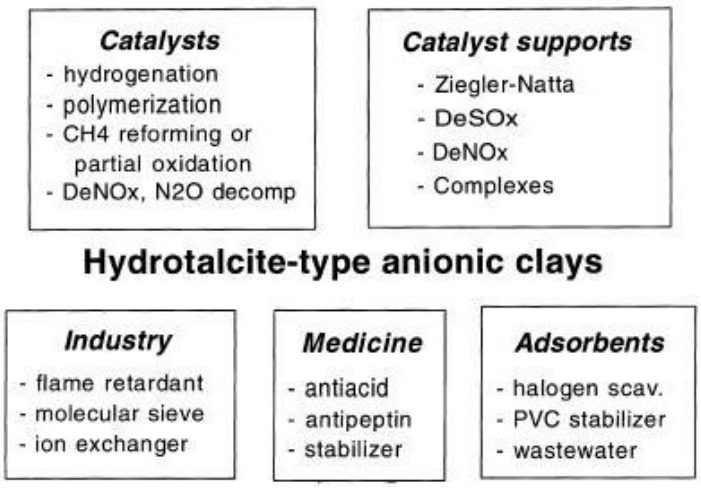

Figure 9: Application of Hydrotalcite like compounds [69]

Their basic properties, high surface area and formation of homogeneous mixture of oxides after calcination finds application also in the field of catalysis. The “Memory effect” property of these compounds find application in the field of water treatment, anion exchangers, etc. [69].

2.4.2. Clay Materials

Man has been using clay for centuries and it is one of the most common minerals on Earth. Historic records reveal that as long ago as 25000 years, primitive people in Europe and Asia have been using clay to produce pottery, figures and other household materials. Clay minerals and clays constitute the world’s largest and most used material with versatile features. Clay materials can be classified into two main categories: cationic clays and anionic clays. Cationic clays are widespread in nature; they have negatively charged alumino-silicate layers, which have cations in the interlayer space to balance the charge. Anionic clays are rare in nature but are relatively inexpensive and simple to synthese. They are characterized by positively charged metal hydroxide layers with balancing anions and water molecules located interstitially [70].

2.4.2.1. Anionic clays

Anionic clays are natural or synthetic lamellar mixed hydroxides with interlayer spaces containing exchangeable anions. Table 2 gives a list of some natural anionic clays, its composition, crystallographic parameters and symmetry.

Table 2: Composition, crystallographic parameters and symmetry for some natural anionic clays [71]

Mineral	Chemical composition	Unit cell parameters		Symmetry
		a (nm)	c (nm)	
Hydrotalcite	$Mg_6Al_2(OH)_{16}CO_3.4H_2O$	0.3054	2.281	3R
Manasseite	$Mg_6Al_2(OH)_{16}CO_3.4H_2O$	0.31	1.56	2H
Pyroaurite	$Mg_6Fe_2(OH)_{16}CO_3.4H_2O$	0.3109	2.341	3R
Sjùgrenite	$Mg_6Fe_2(OH)_{16}CO_3.4H_2O$	0.3113	1.561	2H
Stichtite	$Mg_6Cr_2(OH)_{16}CO_3.4H_2O$	0.31	2.34	3R
Barbertonite	$Mg_6Cr_2(OH)_{16}CO_3.4H_2O$	0.31	1.56	2H
Takovite	$Ni_6Al_2(OH)_{16}CO_3.4H_2O$	0.3025	2.259	3R
Reevesite	$Ni_6Fe_2(OH)_{16}CO_3.4H_2O$	0.3081	2.305	3R
Meixnerite	$Mg_6Al_2(OH)_{16}(OH)_2.4H_2O$	0.3046	2.292	3R
Coalingite	$Mg_{10}Fe_2(OH)_{24}CO_3.2H_2O$	0.312	3.75	3R

2.4.3. Hydrotalcite type compounds – Anionic clays

Hydrotalcite (HT) belongs to the category of anionic clays. Hydrotalcite is magnesium/aluminium hydroxylcarbonate layered material which can be easily crushed into white powder. It was first discovered in Sweden in 1842. The stoichiometry of HT, $[Mg_6Al_2 (OH)_2] CO_3.4H_2O$, was first correctly determined by Manasse in 1915, who was also the first to recognize that carbonate ions were essential for its structure. In 1930 Aminoff and Broome recognized the existence of two polytypes of HTs with rhombohedral and hexagonal symmetry (proposed by Manasse) through X-ray investigation [69]. On the other hand a reference name Layered Double Hydroxides (LDH's) is derived from early works of Feithnecht, who called these compounds ``Doppelschichtstrukturen'' (double sheet structures), hypothesizing a structure with intercalated hydroxide layers [70]. Later, this hypothesis was proved wrong by means of XRD analysis of monocrystals, which showed that all the cations are localized in the same layer, with the anions and water molecules located in the interlayer region [69].

2.4.3.1. Structure

The structure of hydrotalcite like materials, depicted in Figure 10, can be best understood by visualizing the structure of brucite $Mg(OH)_2$. In brucite structure, the Mg^{2+} ion is surrounded by six hydroxyl groups in octahedral coordination and these octahedra are connected through edge sharing to form infinite sheets. These infinite sheets are stacked upon one another to give layered network held through hydrogen bonding [72]. Isomorphic replacement of M^{2+} ions by M^{3+} results in an overall positive charge of the layers. The positive charge is compensated by the intercalation of anion A^{n-} in the interlayer space where water of crystallization also finds the place.

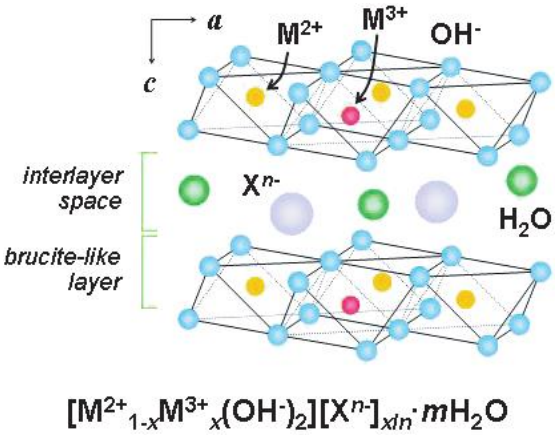

Figure 10: Structure of hydrotalcite like compounds [73]

These materials are characterized by the general formula

$$[M(II)_{1-x}M(III)_x(OH)_2]^{x+}[A^{n-}_{x/n}]^{x-} \cdot mH_2O$$

where M(II) and M(III) are various divalent and trivalent metal ions with $[M(II)_{1-x}M(III)_x(OH)_2]^{x+}$ representing the layer and $[A^{n-}_{x/n}]^{x-} \cdot mH_2O$ representing the interlayer composition, A is the interlayer anion and x = M(III)/M(II)+M(III) can have the values between 0.20 and 0.40 [69,74]. The above formula indicates that it is possible to synthesize various compounds with different stoichiometry. Concerning the value of x, it is possible to obtain pure hydrotalcite like compounds only for the values between $0.2 \leq x \geq 0.33$. For naturally occurring compounds, the value of x is usually 0.25.

M(II) and M(III) cations having an ionic radius not too different from that of Mg^{2+} can form hydrotalcite like compounds. The ionic radii of some of these bivalent and trivalent cations are listed in the Table 3.

Table 3: Ionic radius of cations (Å) [69]

M(II)	Be 0.30	Mg 0.65	Cu 0.69	Ni 0.72	Co 0.74	Zn 0.74	Fe 0.76	Mn 0.80	Cd 0.97	Ca 0.98
M(III)	Al 0.50	Ga 0.62	Ni 0.62	Co 0.63	Fe 0.64	Mn 0.66	Cr 0.69	V 0.74	Ti 0.76	In 0.81

A large number of LDHs have been synthesized with a wide range of M^{2+}/M^{3+} combinations. Table 4 shows selected LDHs with different M^{2+}/M^{3+} combinations reported in various publications.

Table 4: Different M(II)/M(III) chemical composition reported for LDH [74]

M(II)\ M(III)	Al^{3+}	Ga^{3+}	Sc^{3+}	Cr^{3+}	Mn^{3+}	Fe^{3+}	Co^{3+}
Mg^{2+}	X	X	X	X	X	X	X
Ca^{2+}	X	X	X			X	X
Mn^{2+}	X						
Fe^{2+}	X					X	
Co^{2+}	X	X		X		X	X
Ni^{2+}	X	X		X	X	X	X
Cu^{2+}	X			X		X	
Zn^{2+}	X	X		X		X	X

Practically there is no limitation on the type of anion species which can be intercalated into the LDH structure, but the formation of pure or well crystallized materials may become a problem. For example, in the preparation of HTlcs (hydrotalcite like compounds) with anions different from carbonate it is difficult to avoid contamination with CO_2 present in the aqueous solution. The following family of anions have been intercalated [74]:

- halides: F^-, Cl^-, Br^-, I^-
- non-metal oxoanions: BO_3^{3-}, CO_3^{2-}, NO_3^-, $Si_2O_5^{2-}$, HPO_4^{2-}, SO_4^{2-}, ClO_4^-, AsO_4^{3-}, SeO_4^{2-}, BrO_4^-
- oxometallate anions: VO_4^{3-}, CrO_4^{2-}, MnO_4^-, $V_{10}O_{28}^{6-}$, $Cr_2O_7^{2-}$, $Mo_7O_{24}^{6-}$, $PW_{12}O_{40}^{3-}$
- anionic complexes of transition metals (d and f elements): $Fe(CN)_6^{2-}$, Eu (tris-dipicolinte)$^{3-}$, anionic metal porphyrins
- organic anions, R-A^{q-}: A^{q-} = $-COO^-$, $-PO_3^-$, $-SO_3^-$, $-PO_4^{2-}$, $-SO_4^-$
- anionic biomolecules: amino acids, enzymes, proteins, DNA, TPA
- anionic polymers: poly(styrene sulphonate), poly(methyl methacrylate)

The affinity for the interlayer anions can be derived for both mono and divalent anions (the divalent anions are more strongly held in the interlayer than the monovalent anions, and carbonate is held most strongly). The affinity of interlayer anions within the interlayer of hydrotalcite is [75]:

$$CO_3^{2-} >> SO_4^{2-} >> OH^- > F^- > Cl^- > Br^- > NO_3^- > I^-$$

Along with the anions, neutral molecules can also be intercalated giving rise to a wide variety of interlayer compositions [76]. The thickness of the interlayer is determined by the number, size, orientation and the strength of bonds between the anions and the hydroxyl group present in the brucite-like layers.

Water molecules in the interlayer are present in those sites which are not occupied by the anions. The temperature, water vapour pressure and the nature of anions present influences the water content. For instance, HTlc containing nitrates or carbonates may lose one third of its interlayer water at low temperature of about 373K [77]. It has been reported in literature that, as the value of x decreases, the temperature at which the interlayer water is lost is shifted towards lower temperature [78]. It is also possible to calculate the maximum amount of interlayer water on the basis of sites present in the close packed configuration of oxygen atoms, subtracting the sites occupied by the anions.

2.4.4. Preparation methods

Hydrotalcite - like compounds can be synthesized by different methods, such as precipitation at constant pH (also called co-precipitation), precipitation at variable pH, sol-gel, deposition precipitation reactions, structure reconstruction, hydrothermal synthesis, urea hydrolysis reactions and electro chemical methods [79]. Anionic clays are relatively easy and inexpensive to prepare both on laboratory and industrial scales. There are several factors which influences the synthesis of anionic clays. They can be segregated into two categories: structural variables and preparation variables.

Structural variables are [79]:

- Cation size
- x value
- Cation stereochemistry
- Cation mixture
- Nature of the anion

Preparation variables are [79]:

- pH
- Precipitation methods
- Reagent concentration
- Temperature and aging
- Washing and drying
- Presence of impurities

The first step in the process of pure HTlc preparation is to choose the right ratios of cations and anions; these value have to be [69]

$$\mathbf{0.2 \leq [\ M(III)/\ M(II)+M(III)\ ] \leq 0.4}$$

$$\mathbf{1/n \leq A^{n-}\ /\ M(III) \leq 1}$$

The anion which is going to be in the structure of HTlc should be the species present in higher concentration in the solution. In order to avoid the contamination or anion of metal salts entering the structure of HTlc, nitrate salts are usually used.

2.4.4.1. Co-precipitation method

To obtain pure HTlc with high chemical homogeneity, co-precipitation with constant pH method is used [74]. The conditions usually applied are [69]:

- pH in the range of 7-10
- Temperature 333-353 K
- Low concentration of reagents and low flow of the streams

Washing is usually carried out with warm water after some aging, and the drying temperature should not exceed 393K. The pH is kept at a constant level during the reaction by the simultaneous addition of a base solution (NaOH, KOH, etc.) and a mixed metal salts solution.

The structural, chemical and textural properties of the phases are influenced by the pH of co-precipitation. The nature of the solvent in the co-precipitation has a crucial effect on the textural properties of the LDH. This method is well suited to tune the chemical composition of LDH in terms of M(II) / M(III) ratio.

Traditionally, co-precipitation methods are used to prepare large amounts of anionic clays. However, they are not always necessary because of the following reasons:

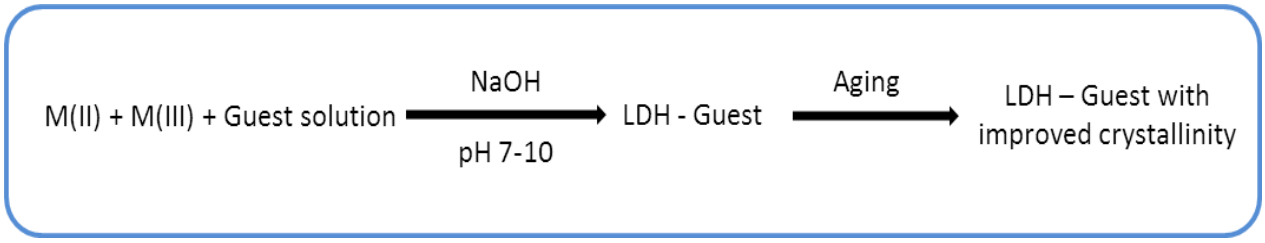

I. in some cases, pure HTlc are not necessary, as the presence of other species may have beneficial effects,
II. the presence in a mixture level outs the differences in the precipitation pH of the single cations, and/or
III. aging and/or hydrothermal treatments may rectify improper precipitation conditions through dissolution/co-precipitation reactions [80].

2.4.4.2. Urea Hydrolysis method

This method was initially developed by Constantino et al. [81] and have undergone several changes since then. A usual preparation procedure for hydrotalcite is as follows: An aqueous stock solution of urea (1.0 M), magnesium chloride (0.1 M) and aluminium chloride (0.1M) are mixed together at the molar Mg/Al/urea ratio of 4:1:10 with magnetic stirring. After cooling to room temperature, the solid precipitate is collected by centrifugation and washed with deionized water subsequently. Urea decomposes on heating of aqueous solution to give ammonia and HNCO. In acidic or neutral media, HNCO is converted into CO_2, and ammonia takes up a proton to give NH_4^+. Both these steps lead to the consumption of H^+ and hence increase the pH of the medium [195, 196]. The so-formed NH^{4+} precipitates the metal nitrates [82].

Usually this method is used for the preparation of carbonate intercalated LDH, but under suitable conditions preparation of nitrate LDH is also possible.

2.4.4.3. Other methods

Apart from these two methods, there are several other methods as listed before. Since the other methods are not often used, they are not discussed here. As pointed out in literature, every LDHs needs specific preparation procedure to be obtained in the best way possible [83].

2.4.5. Thermal decomposition of LDHs

The thermal decomposition of LDHs gives rise to mixed oxides which find many application in industry [69]. This process removes the interlayer water, hydroxyl groups and interlayer anions. The transitions depend on many factors, such as type and relative amount of cations, type of anions, crystallinity and heating atmosphere [70]. Temperature of around 370-570 K characterizes the loss of interlayer water and further, at higher temperature results in the loss of hydroxyl groups from the brucite-type layer and the anions. The resulting material is a homogeneous mixture of metal oxides with a high surface area [69,84]. It was shown that the structure of the LDHs destroyed during calcination can be reconstructed by rehydrating the calcined sample in aqueous solution of appropriate anion. This property of hydrotalcite is called “Memory Effect” [69,85].

Mixed oxides which are obtained after calcination have the following properties [69,70]:

1. High specific surface area (100-300 m^2/g).
2. Synergetic effects between the elements, due to the intimate interdispersion, which favors, for example, the development of unusual basic or hydrogenating properties. It is worth noting that basic properties depend significantly on the composition, as well as calcination temperature.
3. Homogeneous interdispersion of the elements thermally stable also in reducing conditions, with the formation of very small and stable metal crystallites. Impregnation procedures for the preparation of metal catalysts normally cannot achieve such high metal dispersion.
4. Memory effect, which allows reconstruction under mild conditions of the original structure by contact with solutions containing various anions.

Properties 1, 2 and 3 have found applications in the field of catalysis (such as hydrogenation, polymerization, reforming, catalysts support, etc.) whereas properties 1, 2 and 4 have found applications in water treatment, anion exchangers, etc.).

Because of these various advantages, the study of hydrotalcite derived materials has got considerable attention as a potential catalyst precursor for the methanation of carbon dioxide. However, till date only a few publications deal with the CO_2 methanation using hydrotalcite derived catalysts [62]. This work involves the study of CO_2 methanation using Ni- Hydrotalcite derived catalysts.

3. Experimental

3.1. Synthesis of catalysts

Hydrotalcite – like catalysts containing trivalent metal (Al) and divalent metals (Mg, Ni) with different ratios of x (Al/Mg+Ni+Al) and different Ni content were prepared by co-precipitation method at constant pH. Two aqueous solutions, one containing sodium hydroxide (1 M) and the second containing mixed nitrates of divalent and trivalent metals, were added drop-wise into a flask containing an aqueous solution of sodium carbonate and kept under vigorous stirring at 65°C and constant pH of 9.5–10. The mixture was subjected to aging for 24 h and then filtered and washed with deionized water. Then it was dried overnight at 80°C. A pure sample of Mg-Al hydrotalcite (without Ni) was also prepared by the same method.

In order to compare the different samples synthesized in the present work, catalysts were divided into two groups. The first group (Table 5) includes the samples with different Ni percentage and the same M(III)/M(II)+M(III) molar ratio. In these catalysts, Al content was kept constant and Mg atoms were exchanged partly with Ni. The second group (Table 6) contains two catalysts prepared using the same Ni content and exchanging Mg partly by Al atoms.

Table 5: Catalysts studied for the evaluation of Ni content effect. The compositions were determined by ICP analysis.

Catalyst designation	Ni	Mg	Al	x=Al/(Mg+Ni+Al)
$HT_{0.26}$	0.0	33.5	13.0	0.26
13%Ni/$HT_{0.26}$	13.0	23.0	11.0	0.26
17%Ni/$HT_{0.26}$	17.0	21.5	11.0	0.26
20%Ni/$HT_{0.26}$	20.0	20.0	11.0	0.26

Table 6: Catalysts studied for the evaluation of Al/(Mg+Ni+Al) molar ratio effect. The compositions were determined by ICP analysis.

Catalyst designation	Ni	Mg	Al	x=Al/(Mg+Ni+Al)
20%Ni/$HT_{0.26}$	20.0	20.0	11.0	0.26
20%Ni/$HT_{0.20}$	20.0	22.0	8.5	0.20

Prior to catalytic tests, all samples were calcined at 500°C for 5 hours at the rate of 10°C/min, as schematically shown in Figure 11. The samples were also reduced at a temperature chosen through characterization techniques. In addition to the prepared samples, a commercial Ni/Al_2O_3 catalyst with 25wt% Ni is used for comparative studies.

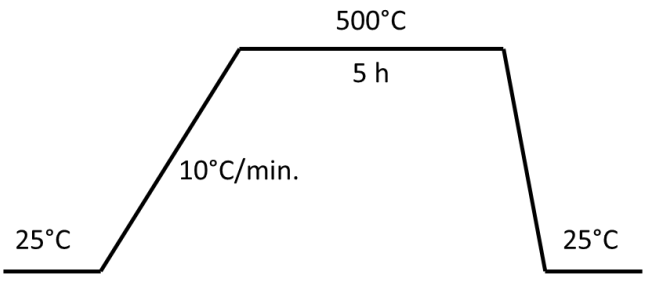

Figure 11: Temperature profile of calcination

3.2. Characterization of the catalysts

The prepared catalyst samples were characterized by ICP analysis, Fourier Transform Infrared (FTIR) spectroscopy, Thermogravimetric Analysis (TGA), XRD, N_2 - Adsorption, H_2- Temperature Programmed Reduction, H_2- Temperature Programmed Desorption, CO_2- Temperature Programmed Desorption and Scanning Electron Microscopy (SEM).

3.2.1. FTIR

Fourier Transform Infrared (FT-IR) spectroscopy is a simple, fast and inexpensive analytical technique which is used for the chemical compound analysis and it is based on the determination of the interaction between an IR radiation and a sample that can be solid, liquid or gas. This method measures the frequencies at which the sample absorbs, and also the intensities of these absorptions. The measured frequencies are helpful for the identification of the sample's chemical composition due to the fact that the bonds between the functional groups are responsible for the absorption of radiation at different frequencies. The spectrum is a two-dimensional plot in which the axes are represented by intensity and frequency/wavelength of sample absorption.

Fourier-transform–infrared spectra were obtained for fresh catalysts with a PerkinElmer FT–IR spectrometer. Thirty-two scans were taken for each spectrum for wave numbers from 400 cm^{-1} to 4000 cm^{-1} registered with a resolution of 4 cm^{-1}. The hydrotalcite samples were mixed with KBr at 1:100 ratio and pressed into disks.

3.2.2. Thermogravimetric analysis (TGA)

The Nomenclature Committee of the International Confederation for Thermal Analysis and Calorimetry (ICTAC) has given the official definition of thermogravimetry as "a technique in which the mass of a substance is measured as a function of temperature whilst the substance is subjected to a controlled temperature program" [66]. It is the most widely used experimental technique for determining thermal changes of solids. It is an advantageous method since it gives quickly the general information regarding the thermal behavior and requires only a small amount of sample. The sample is exposed to an atmosphere of specified composition and temperature [86]. Measurements in either inert or reactive gases, or even in vacuum, are possible over a wide temperature range with a constant heating rate or using different non-linear temperature programs. The derivative thermogravimetry (DTG) gives the mass loss of the sample whereas the differential thermal analysis (DTA) is based on the measurement of temperature difference between the sample and the inert material (reference material) during a temperature program [66].

In this MSc thesis, the experiments were carried out in SETSYS Evolution- SETARAM analyzer. About 40mg of sample used in each test was heated from room temperature to 900°C under air flow at a heating rate of 10° C/min.

3.2.3. X-Ray Diffraction

X-ray diffraction provides a convenient and practical means for the qualitative identification of crystalline compounds. It allows the determination of details of the structure of a solid, as well as its crystallinity or distortions of framework, such as dislocations, grain boundaries, superstructures,

stacking, faults and order-disorder effects. Every crystalline substance has it is own unique X-ray diffraction pattern [66].

Bragg diffraction occurs when radiation is scattered by the atoms of a crystalline material, and undergoes constructive interference. When the scattered waves interfere constructively, they remain in phase since the pathway is equal to an integer multiple of the wavelength. The pathway difference between two waves undergoing interference is given by Bragg's law:

$$2dsin\theta = n\lambda$$

Where:

- d is the interplanar distance
- n is a positive integer
- λ is the wavelength of incident wave
- θ is the diffraction angle

In the present work, XRD measurements were obtained using Bruker AXS Advance D8 diffractometer, using Cu Kα radiation, operating at 40 kV and 40 mA. XRD data were collected between 3 and 90° (2θ) with a step size of 0.03°/16s.

3.2.4. Low temperature nitrogen sorption

Low temperature nitrogen sorption is the most widely used technique to determine catalyst specific surface area and to characterize its porous texture. Sorption isotherms are obtained by plotting nitrogen adsorbed volume against its relative pressure. Based on the solid porous structure, the shape of the isotherm varies. According to IUPAC, six types of isotherms are distinguished but only four, which are shown in Figure 12, are usually found in catalyst [87].

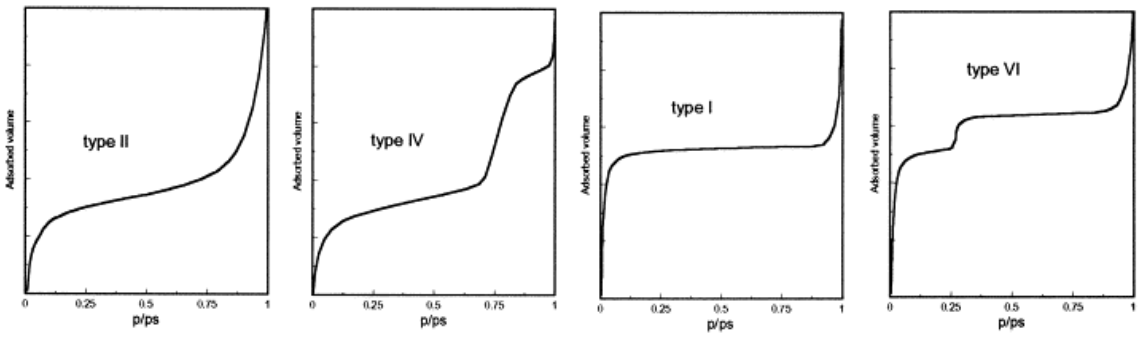

Figure 12: Isotherms obtained through N_2 sorption[87]

The types of isotherms are:

- Macroporous solids - type II
- Mesoporous solids - type IV
- Microporous solids - type I and
- Uniform ultra-microporous solids - type VI.

The BET model developed by Brunauer, Emmet and Teller still remains the most useful tool to determine the monolayer volume (V_m) of the adsorbate, and the specific surface area (A_s). It is given by the equation:

$$A_s = (V_m / 22414)\, N_a \sigma$$

where N_a is Avogadro number and σ is the area covered by one nitrogen molecule. The σ value generally accepted is 0.162 nm^2

In the present work, N_2 – sorption experiments were performed at -196 °C using 200 mg of samples in Quantachrome Autosorb iQ station. The samples were previously outgassed at 90°C for 1 h and then at 300°C for 4 h in flowing nitrogen.

3.2.5. H_2 - Temperature Programmed Reduction

One of the widely used techniques for the characterization of metal oxides, mixed metal oxides and metal oxides dispersed on a support is H_2-TPR. It gives a useful information about the reducibility of the metal species present in the catalyst. In this method, a reducing gas (usually H_2) is passed through a bed of catalyst while temperature is increasing and the consumption of the gas is continuously analyzed through TCD. The consumption of hydrogen as a function of temperature forms a TPR profile. From the TPR profile the ability of the metal species to be reduced, kind of reducible species present in the catalyst, as well as the amount of metal reduced may be determined.

H_2-TPR experiments were carried out in a Micromeritics AutoChem II. For every test, 150 mg of catalyst was used following the temperature profile displayed in Figure 13. Before reduction, the catalyst samples were pre-treated under argon flow (25 cm^3/min) at 250°C for 60 min and then cooled down to room temperature. Reduction of catalysts was carried out in a 30 cm^3/min flow of H_2 (5 vol%)/Ar mixture. The temperature was raised from room temperature to 900°C at the rate of 10°C/min.

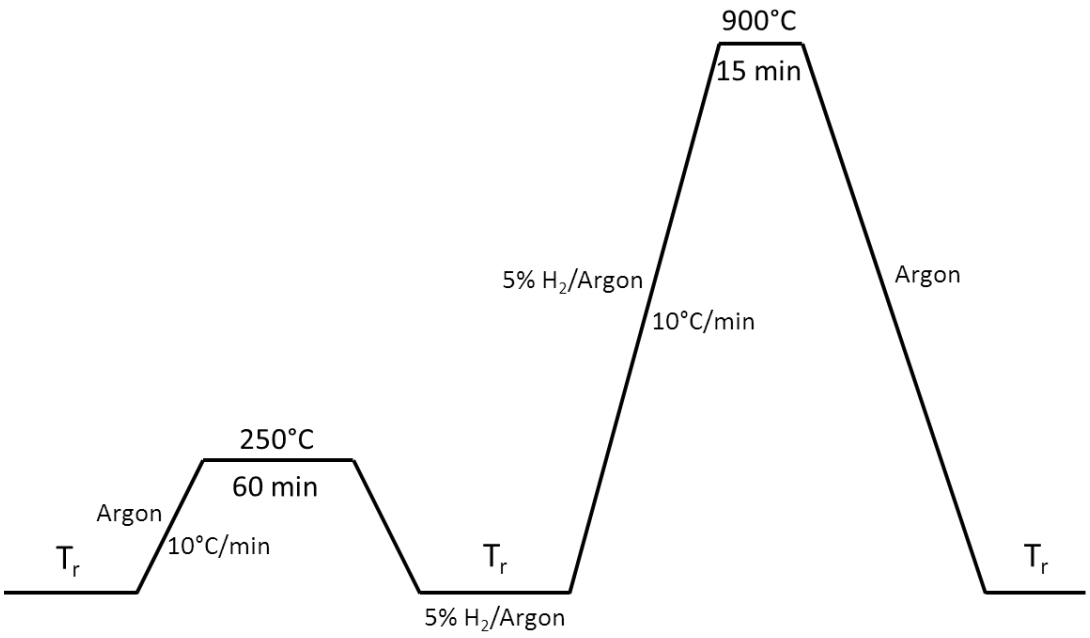

Figure 13: TPR Profile

3.2.6. H_2 - Temperature Programmed Desorption

H_2-TPD is a useful technique for the characterization of metal based catalysts which provides useful information such as metal surface area, dispersion and crystallite size. During the analysis, the sample which is appropriately pre-treated, is exposed to an increasing temperature with a constant rate and is swept by an inert gas such as helium, argon or nitrogen. The gas chemisorbed on the sample surface is desorbed and a suitable detector monitors the process. The detectors commonly used a Thermal Conductivity Detector or a Mass Spectrometer [88].

In this work, H_2-TPD experiments were carried out in a Micromeritics AutoChem II, using 150 mg of catalyst following the temperature profile displayed in Figure 14. From the area of TCD signal, the metal surface area, crystallite size and dispersion were calculated.

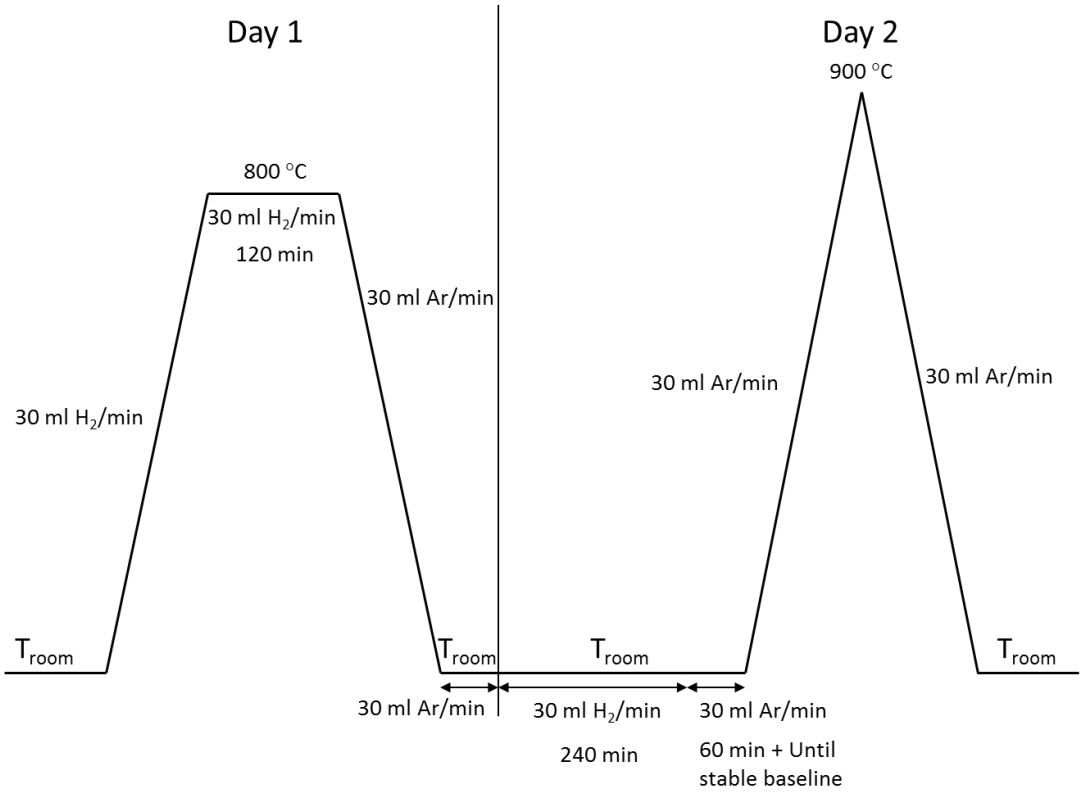

Figure 14: TPD profile

3.2.7. CO_2-Temperature Programmed Desorption

CO_2-TPD was carried out in a fixed-bed flow reactor. The catalyst (m= 0.1744 g approx.) was reduced in-situ at 470 °C for 1 h under 5%H_2/Ar flow of 300 ml/min. It was then cooled down to ambient temperature under the same atmosphere. Then, the gas mixture was changed for 1 h to 14%CO_2/Ar flow of 175 ml/min. After that, CO_2 was closed and excess adsorptive gas was purged with Ar flow of 150 ml/min, until a constant baseline was established in the program. Once the baseline was established, the catalyst was heated up to 500 °C at a rate of 10 °C /min in the Ar flow, and the desorbed species were analyzed using ABB EL3020 CO_x analyzer.

3.2.8. Scanning Electron Microscopy (SEM) and Transmission Electron Microscopy (TEM)

The morphology of the synthesized catalytic samples was observed using SEM. It involves scanning a fine beam of electrons over a specimen and detecting the signals which are emitted. The resolution of SEM images is better than that of conventional optical microscope but less than that of TEM. SEM characterization technique has become widely popular because of its features such as ease of operation, relaxed requirement for specimen preparation, excellent 3-D views of complex catalytic surfaces and its outstanding deep of field [89]. Experiments were carried out at *Universidade de Aveiro* using a Hitachi TEM H9000 equipment operating at 300kV.

3.3. Catalytic Tests

The catalytic tests were carried out in a catalytic unit schematically shown in the Figure 15

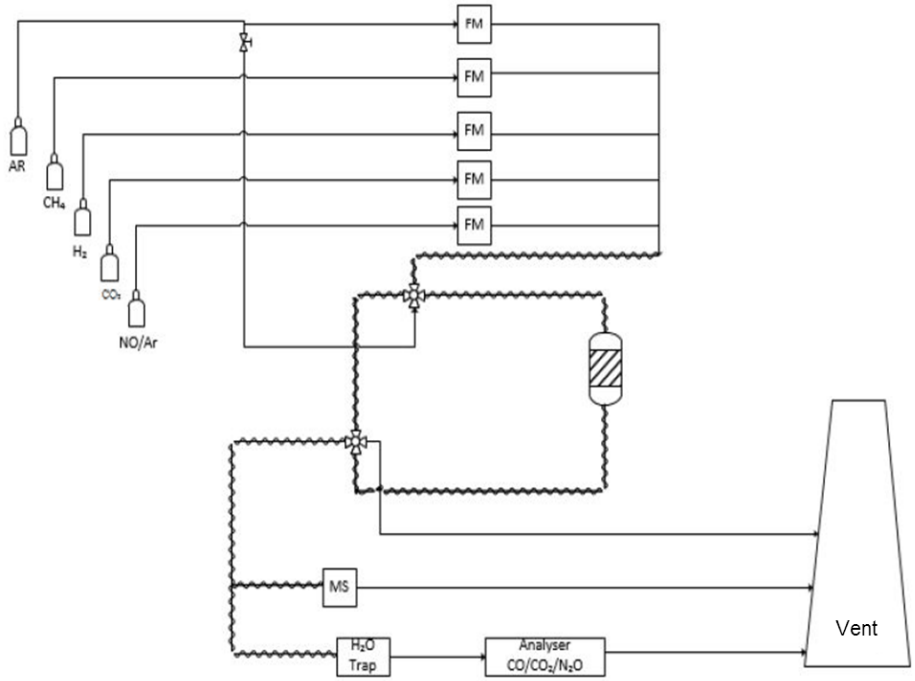

Figure 15: Scheme of the catalytic unit used in the experiments

The prepared samples were tested in order to study the difference in the conversion of CO_2 and the selectivity to CH_4 as a function of reaction temperature. All catalytic tests were carried out in a fixed bed reactor under atmospheric pressure. The reactor was heated using a TermoLab Fornos Eléctricos oven with a temperature controller. A thermocouple was placed outside and close to the reactor bed to follow the reaction temperature during the tests. All gases used throughout the tests were supplied by Air Liquid and had purity above 99.999%.

All the samples were reduced ex-situ at 800 °C under pure H_2 flow. Before the tests, all samples were pre-reduced in-situ at 470 °C for one hour using 300 ml/min flow of 5% H_2/Argon stream. They were then cooled down to 200 °C. After the pre-reduction, the reactivity tests were carried out using the feed constituted of hydrogen, carbon-dioxide and argon at a molar ratio of 4:1:95

and a total flow of 300 ml/min with GHSV of 15000 h^{-1}. The hydrogen, carbon dioxide and argon flows were controlled by calibrated mass flow Brooks controllers. The mass of the catalyst was kept constant (0.1744g) for all the tests. The reaction was carried out in the temperature range of 200 °C to 450 °C in steps of 50 °C with the heating rate of 5 °C/min. In each step the temperature was kept constant for 45 minutes. The amounts of CO, CO_2 and CH_4 at the reactor outlet were analyzed using an ABB EL3020 CO_x and CH_4 analyzers. CO, CO_2 and CH_4 are measured every 5 seconds and at each temperature, after the stabilization of the signal an average value was calculated. The temperature profile of the pre-reduction in-situ and catalytic tests is shown in the Figure 16.

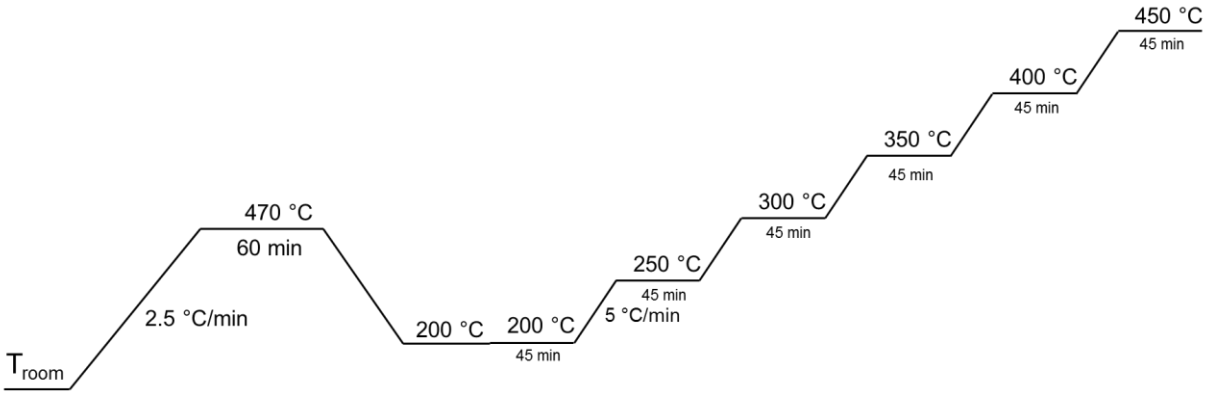

Figure 16: Temperature profile of Pre-reduction and catalytic test

Conversion of CO_2 was calculated using the equation:

$$x = \frac{n_{in\,CO_2} - n_{ef\,CO_2}}{n_{in\,CO_2}} \cdot 100\%$$

n_{inCO2} – inlet molar flow of CO_2 [mmol/min]

n_{efCO2} – effluent molar flow of CO_2 [mmol/min]

Selectivity to methane was determined as:

$$S = \frac{C_{CH4}}{C_{CH4} + C_{CO}} \cdot 100\%$$

C_{CH4} – concentration of methane [ppm]

C_{CO} – concentration of carbon monoxide [ppm]

4. Results and discussion

As reported in section 3.1, the samples were divided into two categories, one with different Ni content and other with different x (x= Al/Al+Mg+Ni). The characterization techniques and catalytic performances were studied for these groups.

4.1. Nickel content effect

In this section, the results of the characterization techniques and catalytic test of samples with different Ni content (Table 5) were studied and analyzed.

4.1.1. Catalysts characterization

To start the study, **FTIR** characterization was performed for the non-calcined samples (Figure 17). As it can be observed, the same bands are present in all the spectra of the different samples. The first band around 3500-3600 cm^{-1} can be attributed to the H-bonding stretching vibrations of the OH group in the brucite-like layer [69]. In addition, a shoulder can be observed around 3000 cm^{-1}. This has been attributed to hydrogen bonding between H_2O and the anion in the interlayer [69] being an additional band of H_2O bending vibration present at 1600 cm^{-1}. Furthermore, the main absorption bands of the anions are observed between 1000 and 1800 cm^{-1} being reported carbonate bands at 1350-1380 cm^{-1}, 850-880 cm^{-1} and 670-690 cm^{-1} [69]. As a conclusion, FTIR studies confirm that hydrotalcite materials were synthesized by the experimental procedure carried out.

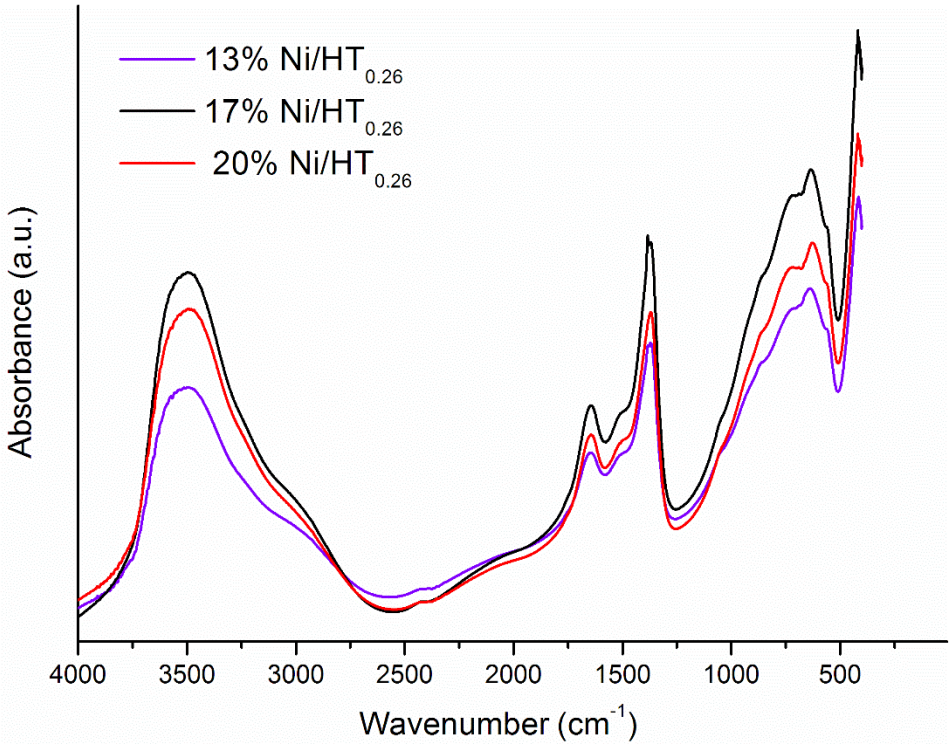

Figure 17: FTIR spectra obtained for non-calcined samples with different Ni content.

FTIR studies were followed by **thermogravimetric** studies carried out for all the non-calcined samples (Figure 18). As it can be observed, the $HT_{0.26}$ as well as the samples with different Ni contents present two main transitions: the first below 350ºC and the second above 350ºC. As reported in the literature [69], the thermal behavior of hydrotalcite-like materials is characterized by these two transitions. The first one, endothermic and at temperatures from 100 to 300ºC, corresponds to the loss of interlayer water, without collapse of the structure. This step is reversible. The second step, endothermic, at temperatures from 350 to 500ºC, is due to the loss of hydroxyl groups from the brucite-like layers, as well as of the anions [69]. However, the first and second transition seems to present more than one stage for all catalysts shown in Figure 18. This could be attributed to different kinds of interlayer water for the first transition and to the loss of the hydroxyl groups bound to Al and Mg as well as carbonates decomposition in the second one, as already reported in the literature [69]. In terms of quantification of mass loss, all samples of the present study reached ~45% at 900ºC, which is in accordance with literature findings [90]. The results obtained from thermogravimetric studies confirm that a temperature of 500ºC should be used for the calcination treatment in order to complete all the decomposition processes. The effect of calcination and reduction in some selected samples will be discussed in Section 4.3.1.

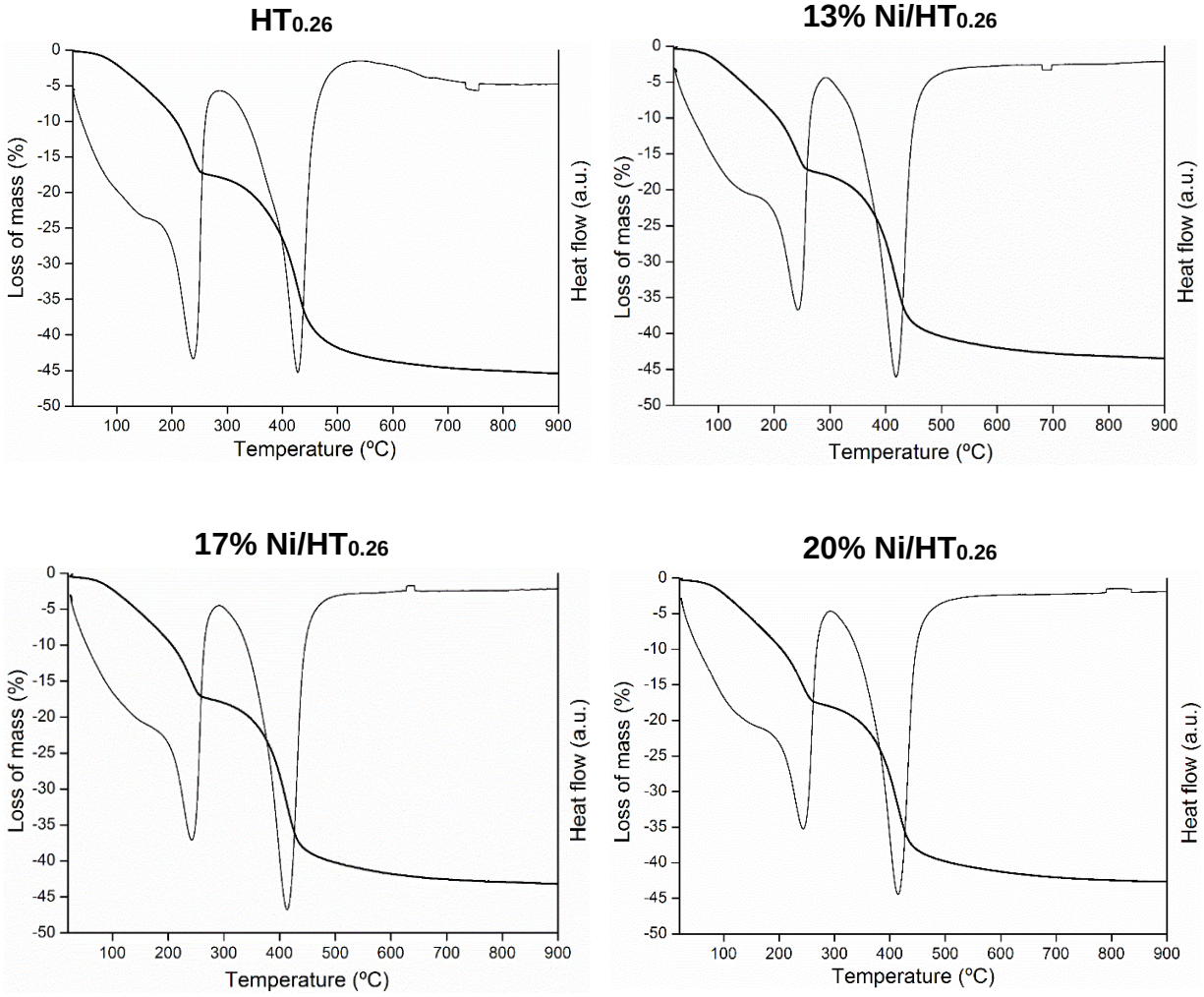

Figure 18: TGA profiles of non-calcined samples with different Ni content.

The **XRD** patterns of the samples prepared for the study of the Ni content effect are shown in Figure 19. As it can be observed, the non-calcined samples show some general features already reported for hydrotalcite materials [69], namely, the presence of sharp and intense lines at low values of 2θ angle, and less intense and generally asymmetric lines at higher angular values. These diffraction patterns indicate the good crystallinity of the prepared samples. Three relatively narrow reflection are present at low 2θ values (2θ = 11.6°, 23.2°, 34.8°) corresponding to the (0 0 3), (0 0 6) and (0 1 2) planes of hydrotalcite structure. Regarding the calcined samples, the post-synthesis treatment completely destroys the layered structure of the hydrotalcite, resulting in a high surface area mixed oxides, as it will be discussed in the characterization of the textural properties. As observed in the patterns of the non-calcined samples, no important differences have been observed in the XRD patterns of the samples with different Ni contents. It can be verified that the main reflections observed in the non-calcined samples are replaced by three diffuse lines in the calcined samples (2θ = 35°, 43.5° and 63°), irrespective of the Ni content, which indicate the presence of NiO, $NiAl_2O_4$, MgO and solid solutions of NiO/MgO indicated as $Ni_xMg_{(1-x)}O_2$.

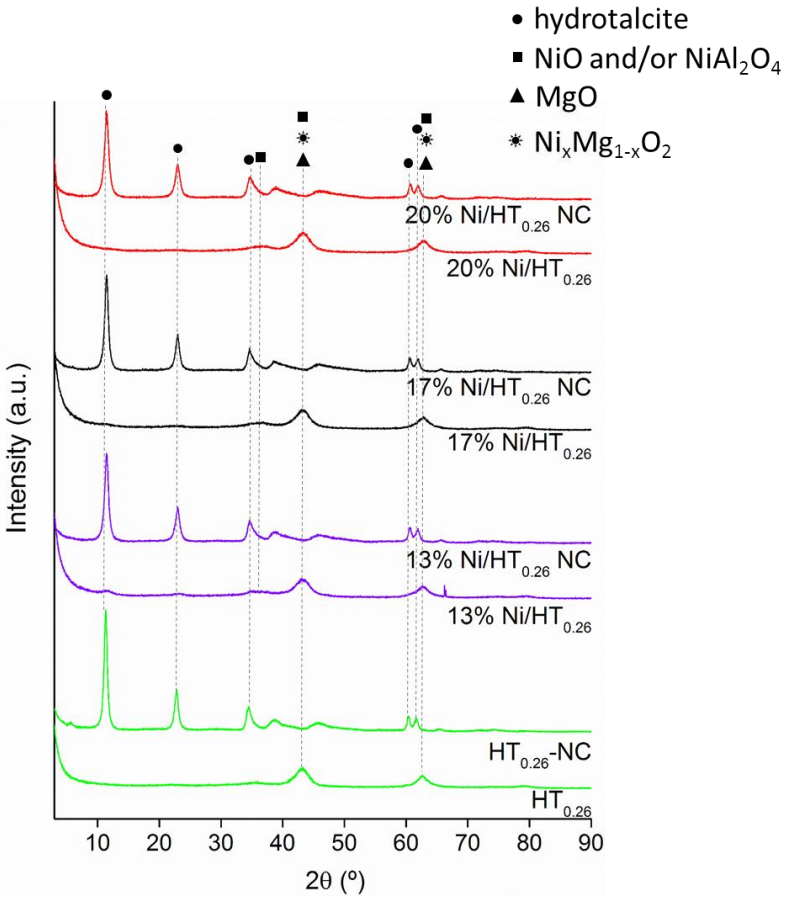

Figure 19: XRD patterns of Ni-HT derived samples. NC denotes sample is not calcined.

In order to characterize the calcined samples in terms of textural properties, **N_2 - sorption** studies were carried out. The isotherms obtained for the different samples are shown in Figure 20. In all cases the adsorption/desorption experiments yielded an isotherm closest in shape to the IUPAC type IV, displaying a marked hysteresis between the adsorption and desorption curves. Isotherms of

this type are characteristic of mesoporous materials, whereby the adsorption at lower values of P/P_0 is consistent with the single-layer/multi-layer adsorption, also found with non-porous materials, whilst the distinct hysteresis at higher values of P/P_0 indicates capillary condensation in the mesopores.

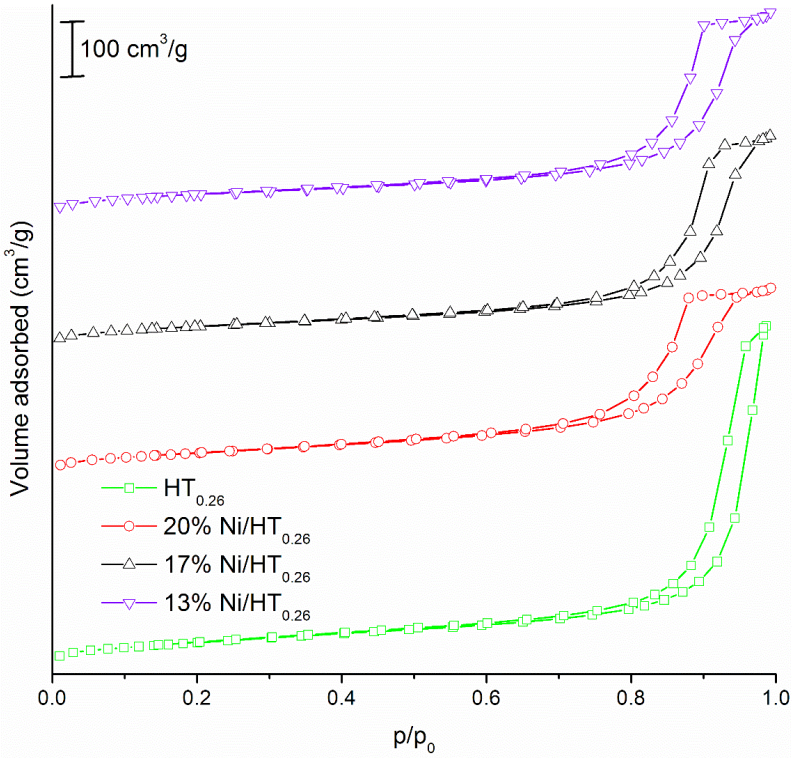

Figure 20: Isotherms obtained for samples with different Ni content.

By the analysis of the data obtained from N_2 adsorption, the main textural properties of the different samples were determined (Table 7). As it can be observed, BET surface areas were not strongly affected by the Ni content and the values are in accordance with the literature [90]. In terms of average pore diameter calculated by BJH method, a decrease with Ni incorporation can be observed. Furthermore, it was verified that the mesoporous volumes were reduced with Ni incorporation and no trend was found for Ni content effect being the results for Ni samples very similar between them. The absence of micropores in these materials was ascertained by the analysis of the t-plots derived from the sorption isotherms.

Table 7: Textural properties determined for calcined samples of the current study.

Catalyst	S_{BET} (m^2/g)[a]	D_p (nm)[b]	V_{meso} (cm^3/g)[c]	V_{micro} (cm^3/g)[d]
$HT_{0.26}$	238	32	0.896	0.018
13% $Ni/HT_{0.26}$	236	20	0.681	0.036
17% $Ni/HT_{0.26}$	223	19	0.721	0.026
20% $Ni/HT_{0.26}$	236	16	0.654	0.011

[a] BET surface area;

[b] Pore diameter determined from the adsorption isotherms by BJH method;

[c,d] Pore volumes determined by t-plot method.

In order to determine the reduction profiles of the samples with different Ni contents, **H_2-TPR** analysis was carried out (Figure 21). The TPR profiles display several peaks around 160, 390 and 860ºC, corresponding to NiO in various states of interaction with the hydrotalcite derived materials. The first two peaks occurring at lower temperatures could be associated with the reduction of segregated NiO as well as NiO weakly interacting with MgO [91]. The third bigger peak could be attributed to the reduction of Ni strongly interacting with the MgO lattice (bulk NiO from NiO/MgO mixed oxides) [92] as well as Ni from $NiAl_2O_4$ [93,94]. The maximum temperature and the area of the peak at temperatures close to 850ºC changes with Ni content. The higher the Ni content the lower the maximum temperature, as has also been previously observed [92]. Thus, the temperature chosen for the reduction treatment carried out prior to the catalytic test was 800ºC.

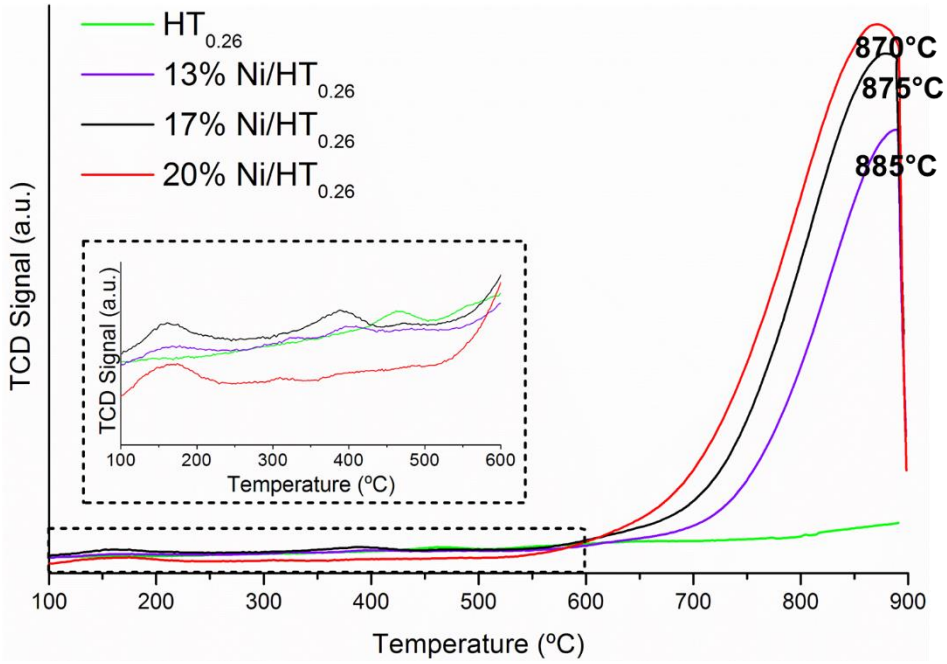

Figure 21: H_2-TPR profiles of samples with different Ni content.

H_2-TPD experiments were carried out in order to evaluate the effect of hydrotalcite derived systems on the nickel dispersion, as well as for the estimation of the average Ni^0 sizes. The profiles obtained for the desorption of H_2 can be found in Figure 22, where it can be observed that even the $HT_{0.26}$ without nickel presents a small H_2 uptake. This could lead to an overestimation of the H_2 uptake attributed to Ni particles in the Ni-HT derived catalysts.

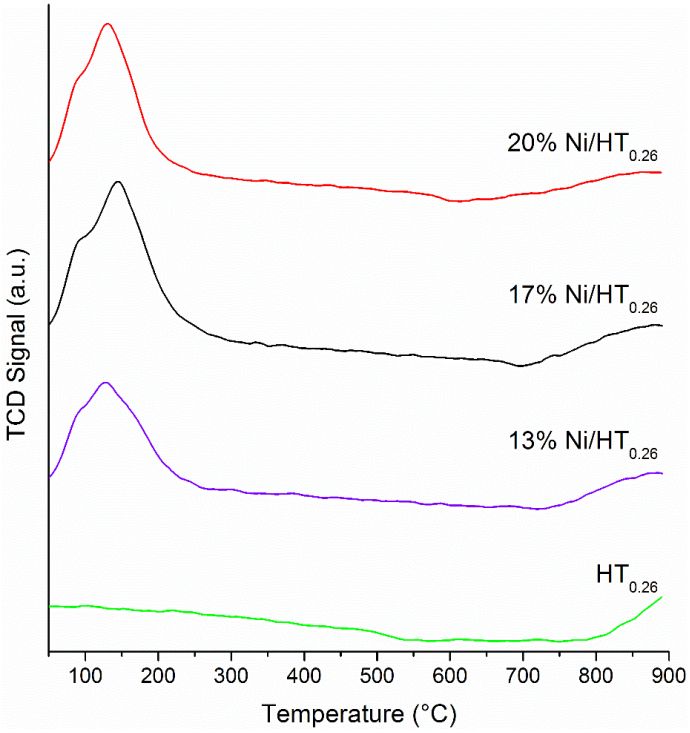

Figure 22: H_2-TPD profiles for samples with different Ni content.

The determined dispersion and estimated Ni^0 sizes can be observed in Table 8. As observed, all catalysts present similar dispersions and no trend can be inferred. In terms of Ni^0 particle sizes, the obtained values are much higher than those reported in the literature [91,95,96]. This could be attributed to the already referred overestimation of H_2 uptake. It can be observed that the sizes are bigger than those obtained for the pore diameters in N_2 adsorption.

Table 8: Dispersion and average metallic Ni particle size derived from H_2-TPD data.

Catalyst	Metal dispersion (%)	Estimated Ni^0 particle size (nm)
13% Ni/$HT_{0.26}$	2.01	51
17% Ni/$HT_{0.26}$	2.41	43
20% Ni/$HT_{0.26}$	1.95	53

In order to characterize the basicity of the catalysts containing Ni in comparison to hydrotalcite sample, **CO_2-TPD** experiments were carried out. Desorption profiles from room temperature to 500ºC can be found in Figure 23. Similar shapes were obtained for all samples with three main peaks attributed to weak, medium and strong basic sites. Weak Brönsted basic sites are associated with surface OH^- groups, medium-strength Lewis sites are related to Mg^{2+}–O^{2-} and Al^{3+}–O^{2-} acid–base pairs and strong Lewis basic sites are due to the presence of low coordinated O^{2-} [97–99]. However,

the maxima temperatures for the peaks related to the three types of basic sites are different for different catalysts.

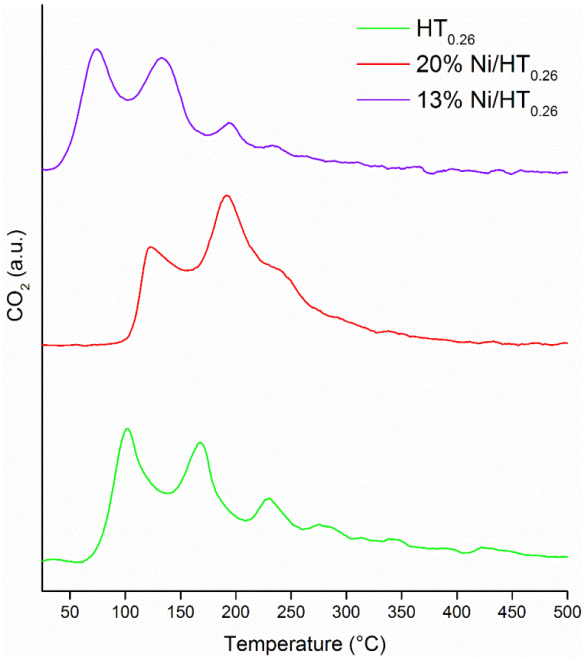

Figure 23: CO_2-TPD profiles for samples with different Ni content.

The contribution of each type of basic sites to the CO2-TPD profile as well as the maximum temperature for each desorption peak can be found in Figure 24. As observed, the higher the Ni content the more important the contribution of strong sites indicating a more pronounced presence of low coordinated O^{2-}.

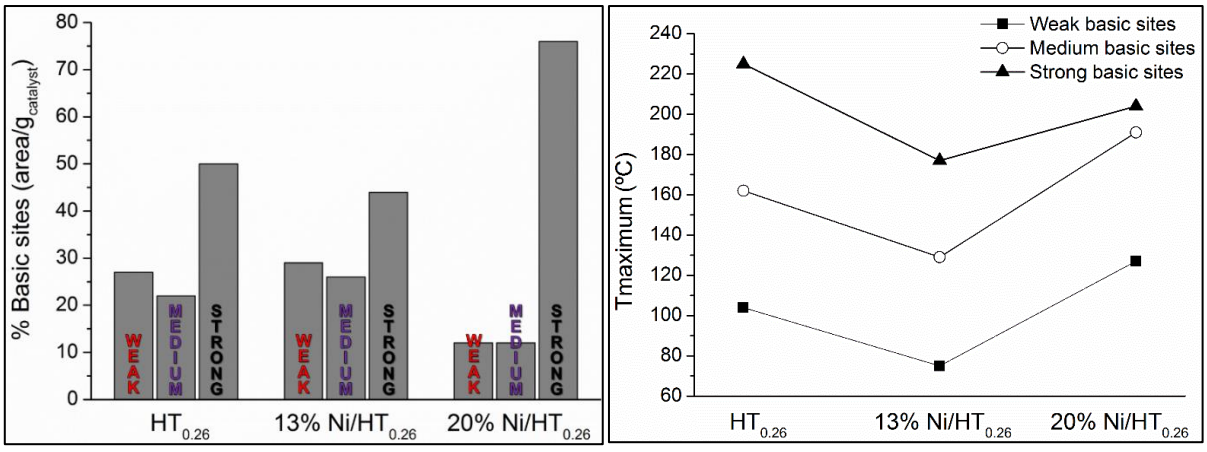

Figure 24: Comparison of different basic sites and maximum temperature for samples with different Ni content

Finally, SEM characterization was carried out in order to obtain information about the morphology of the synthesized catalysts. Figure 25 shows the SEM images for the non-calcined, calcined and reduced samples of $HT_{0.26}$ and 20% $Ni/HT_{0.26}$. The morphology of prepared hydrotalcite catalysts were formed as an accumulation of nano particles aggregates [100]. The crystallinity of samples was good and also in accordance with characteristic reflections appeared from XRD pattern.

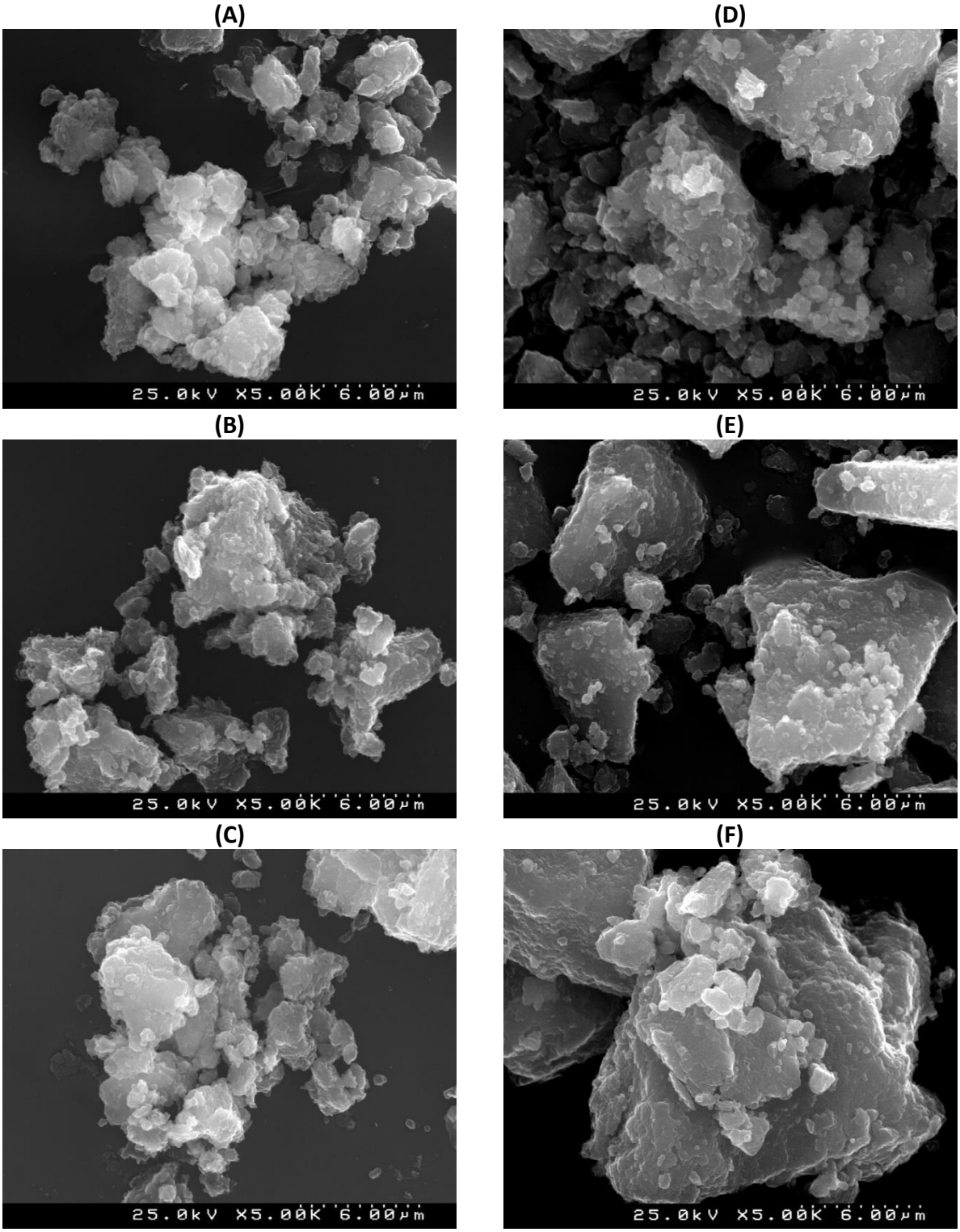

Figure 25: SEM images for $HT_{0.26}$ (A) Non-calcined, (B) Calcined, (C) Reduced and 20%$Ni/HT_{0.26}$ (D) Non-calcined, (E) Calcined, (F) Reduced.

4.1.2. Catalytic tests

The catalytic performances of the samples containing different amounts of Ni can be found in Figure 26. As it can be observed, the $HT_{0.26}$ which is used as reference presents activity towards CO_2 methanation even without Ni. Catalytic performances are close to thermodynamics at temperatures above 350 °C. For catalysts containing increasing amounts of Ni, no significant difference can be observed in terms of both CO_2 conversion and CH_4 selectivity and; the results obtained for the three Ni catalysts are quite similar between them. This could be attributed to the similar characteristics determined in terms of textural properties and Ni dispersion; and also the experimental error of CO_2 conversion and CH_4 selectivity.

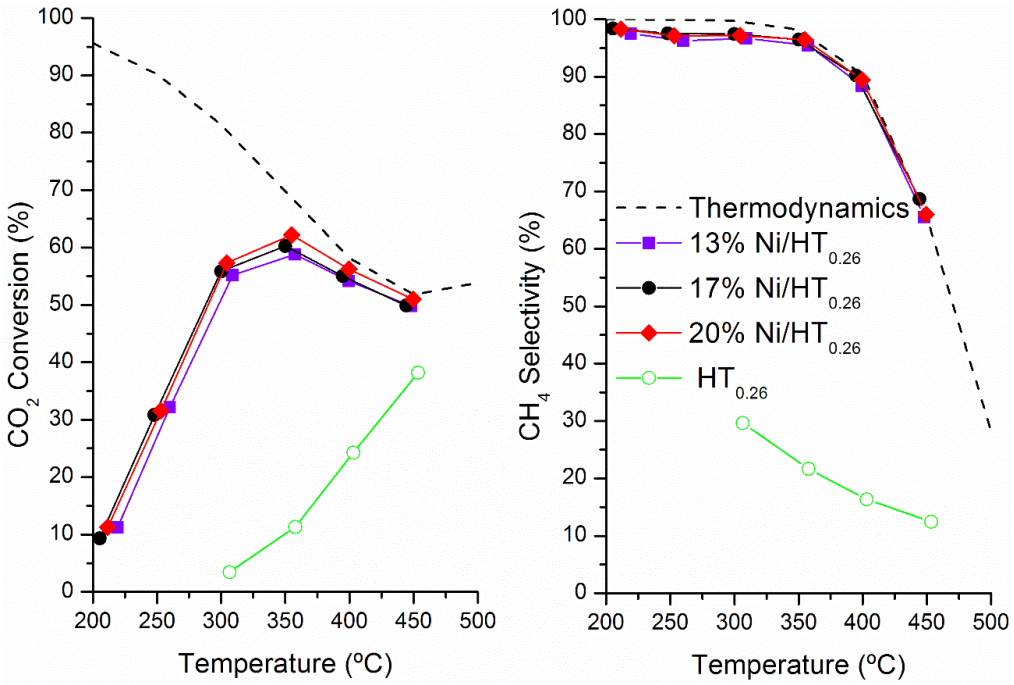

Figure 26: CO_2 conversion and CH_4 selectivity of samples with different Ni content. Conditions: H_2:CO_2:Ar=4:1:95, GHSV=15000 $h^{-1}$and atmospheric pressure

4.1.3. Summary

The main conclusions of the Section 4.1 are summarized in Table 9.

Table 9: Summary of results obtained in Section 4.1.

Technique	Main information inferred
FTIR	HT structure was obtained irrespective of Ni content
TG	The same profile was obtained irrespective of Ni content. Two transitions were observed. The calcination temperature was determined (500ºC)
XRD	HT structure was verified in the non-calcined samples. NiO, $NiAl_2O_4$, MgO and solid solutions of NiO/MgO peaks were detected in the calcined samples
N_2 - sorption	BET surface areas were not strongly affected by the Ni content. Average pore diameters and mesopores volumes decrease with Ni incorporation
H_2-TPR	Main reduction peak above 800ºC shifting to lower temperatures with the increasing Ni content. The pre-reduction temperature was determined (800ºC)
H_2-TPD	No trend was observed in terms of dispersion. Higher Ni content leads to bigger particles
CO_2-TPD	Three type of basic sites irrespective of Ni content
Catalytic tests	Similar results between the samples, slight increase with Ni content. Results very close to thermodynamic values above 350ºC

4.2. Structural effects

In this section, the results of the characterization techniques and catalytic test of samples with different x (x=Al/Al+Mg+Ni) content (Table 6) were studied and analyzed.

4.2.1. Catalysts characterization

The spectra obtained from **FTIR** studies and used for the comparison of the structural effect (Figure 27) are similar to those of the Ni content effect with different bands corresponding to H-bonding stretching vibrations of the OH group in the brucite like layer, hydrogen bonding between H_2O and the anion in the interlayer, vibrations of anion, etc. It can be observed from the graph that there is a shift to higher wavenumbers for some bands with the decreasing x (x=Al/Al+Mg+Ni). This shift is in accordance with the literature findings [69] and has been attributed to the modification in the interlayer spacing.

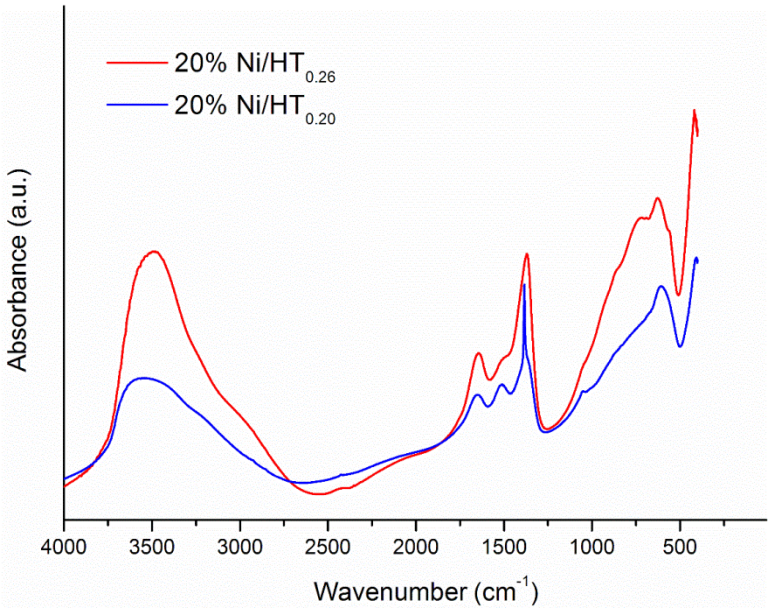

Figure 27: FTIR spectra for samples with different structure composition.

The **XRD** patterns for the study of structural effect are shown in the Figure 28. Taking into account the findings presented in the previous chapter concerning XRD studies, the reflections observed in the different patterns confirm the synthesis of hydrotalcite like materials, no significant changes observed in the patterns obtained for the samples with the different x. As obtained previously for the samples containing different Ni amount, the calcined samples of Ni-HT catalysts with different x displayed the peaks at 2θ ~ 43.5 and 63° corresponding to (2 0 0) and (2 2 0) planes of the periclase-like structure [90].

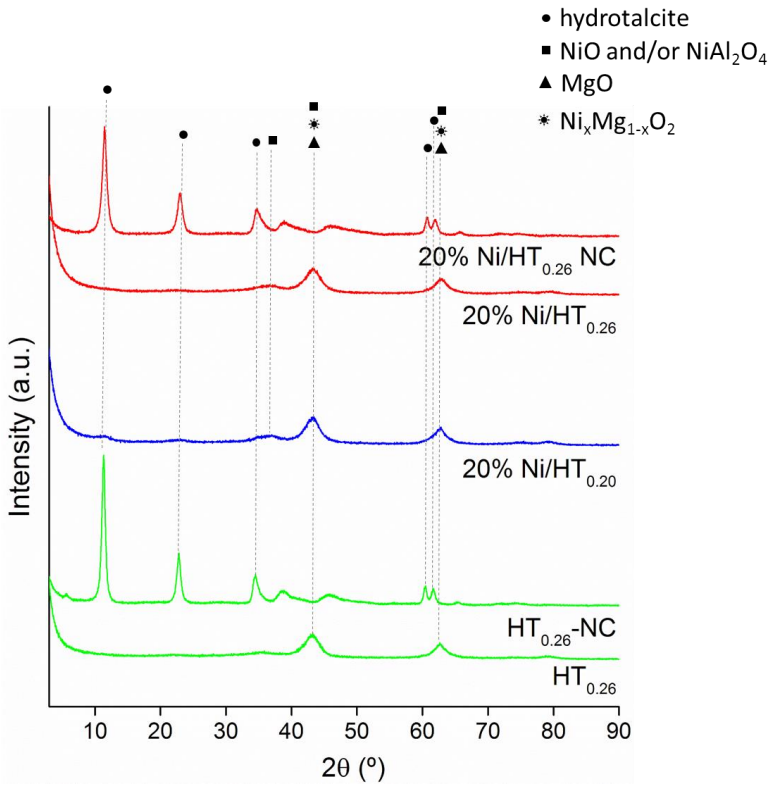

Figure 28: XRD patterns of Ni-HT derived samples. NC denotes sample is not calcined.

The **textural properties** of the samples with different x were determined from low-temperature nitrogen sorption isotherms shown in Figure 29. The isotherms are of IUPAC type IV, characteristic of mesoporous materials.

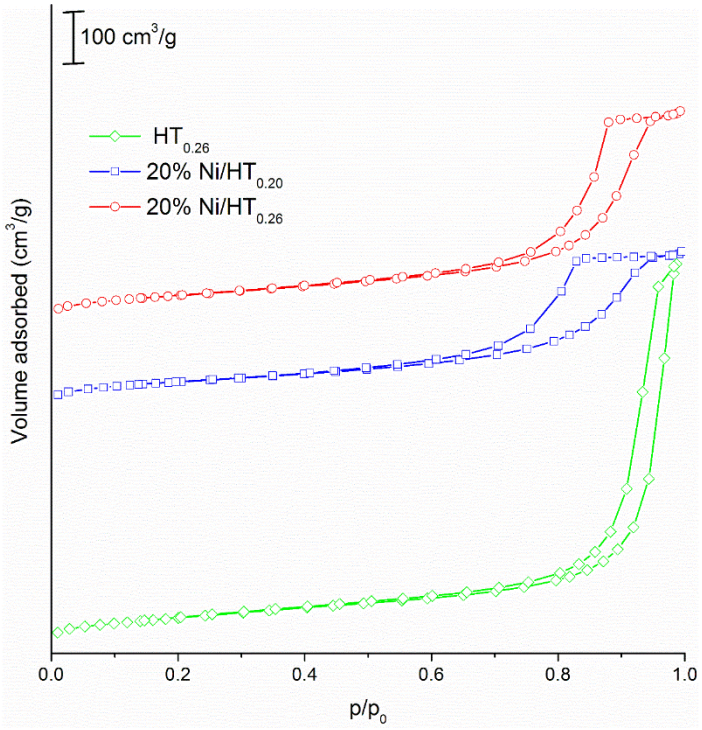

Figure 29: Isotherms obtained for samples with different x.

The textural properties obtained by the analysis of data from N_2 - sorption are displayed in the Table 10. It can be seen that pore diameters and mesoporous volumes slightly increases with x value, as observed in the literature [98]. Higher x factor implies more Al in the structure. As explained in the Literature review (Section 2.4.3.1), the presence of Al generates positive charges in the structure which is compensated by CO_3^{2-} anions in the interlayer. During calcination these carbonates are decomposed generating porosity in the material [98]. A higher amount of carbonates (higher x) in the non-calcined sample leads to higher pore volumes and pore sizes after calcination, in accordance with the results obtained in the present study.

Table 10: Textural properties determined for the calcined samples with different x.

Catalyst	S_{BET} (m^2/g)[a]	D_p (nm)[b]	V_{meso} (cm^3/g)[c]	V_{micro} (cm^3/g)[d]
$HT_{0.26}$	238	32	0.896	0.018
20% $Ni/HT_{0.26}$	236	16	0.654	0.011
20% $Ni/HT_{0.20}$	226	12	0.474	0.019

[a] BET surface area;

[b] Pore diameter determined from the adsorption isotherms by BJH method;

[c,d] Pore volumes determined by t-plot method.

Regarding **H_2-TPR** profiles (Figure 30), lower x in the catalyst leads to a shift to lower temperature of the maximum of the main Ni reduction peak. In addition, the sample with lower x shows a peak around 330ºC which could be attributed to the presence of a higher amount of NiO particles dispersed in the surface of the catalyst.

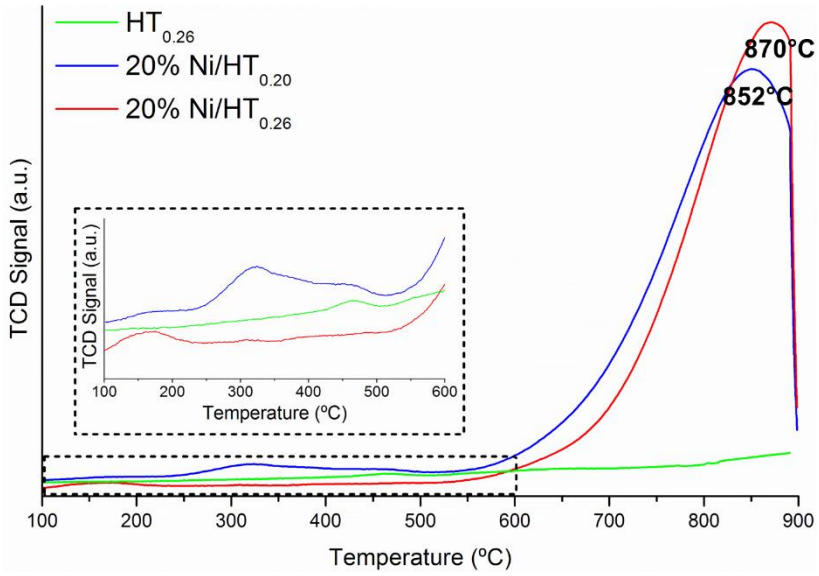

Figure 30: H_2-TPR profiles of samples with different x.

Concerning **H_2-TPD studies**, the profiles of H_2 desorption are represented in Figure 31. As it can be observed, the profiles obtained for the samples with different x are considerably similar where the temperature of maximum is concerned. The only difference is a slightly higher H_2 desorption below 88ºC for the sample with x=0.26.

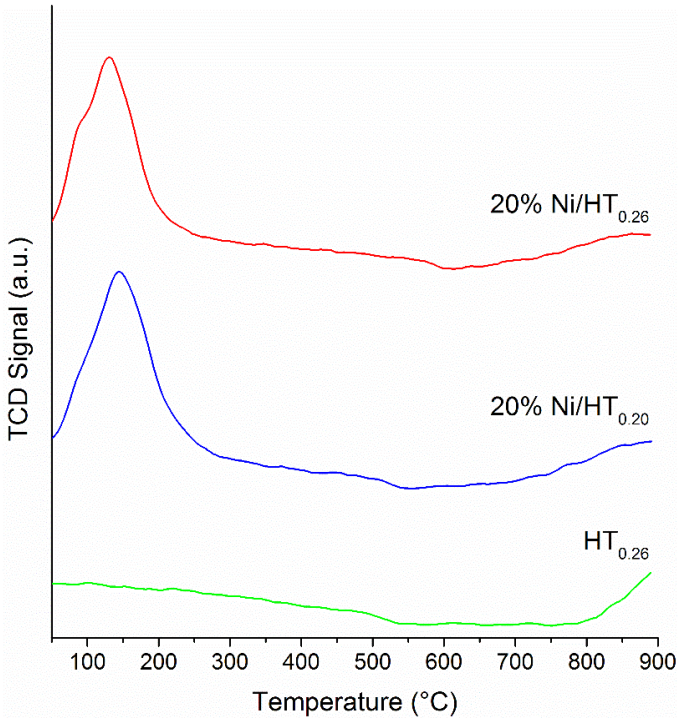

Figure 31: H_2-TPD profiles for samples with different x.

From the analysis of the H_2 uptake, the dispersion of Ni as well as the Ni^0 average particle size was determined (Table 11). Higher x leads to lower dispersion and, as a result, bigger average size for Ni^0 particles.

Table 11: Dispersion and average metallic Ni particle size derived from H_2-TPD data.

Catalyst	Metal dispersion (%)	Estimated Ni^0 particle size (nm)
20% Ni/$HT_{0.20}$	5.83	18
20% Ni/$HT_{0.26}$	1.95	53

CO_2-TPD experiments carried out are shown in Figure 32. Three types of adsorption sites can be observed, similarly as in the previous chapter (section 4.1.1). The desorption temperatures are the same as for the $HT_{0.26}$. When comparing the profiles of samples with different x, it can be noticed that higher x leads to slightly higher CO_2 uptake. The presence of higher amount of Al species in the Mg-based structure (higher x) leads to the generation of additional surface O^{2-} ions suitable for CO_2 adsorption [98] justifying the increase in the CO_2 uptake.

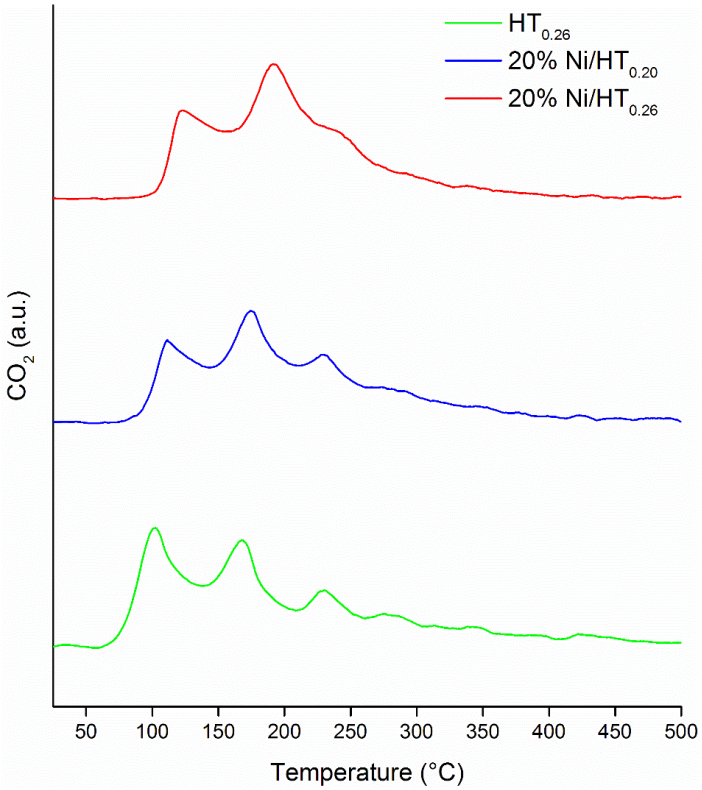

Figure 32: CO_2-TPD profiles for reduced samples with different x.

Regarding the contribution of the different type of basic sites (Figure 33), it can be observed that a higher x value leads to more strong sites. In addition, the maximum temperatures for the different desorption peaks shift with the structure composition. Thus, weak and medium sites maximum temperatures increase with x ratio whereas strong sites maximum temperature decreases.

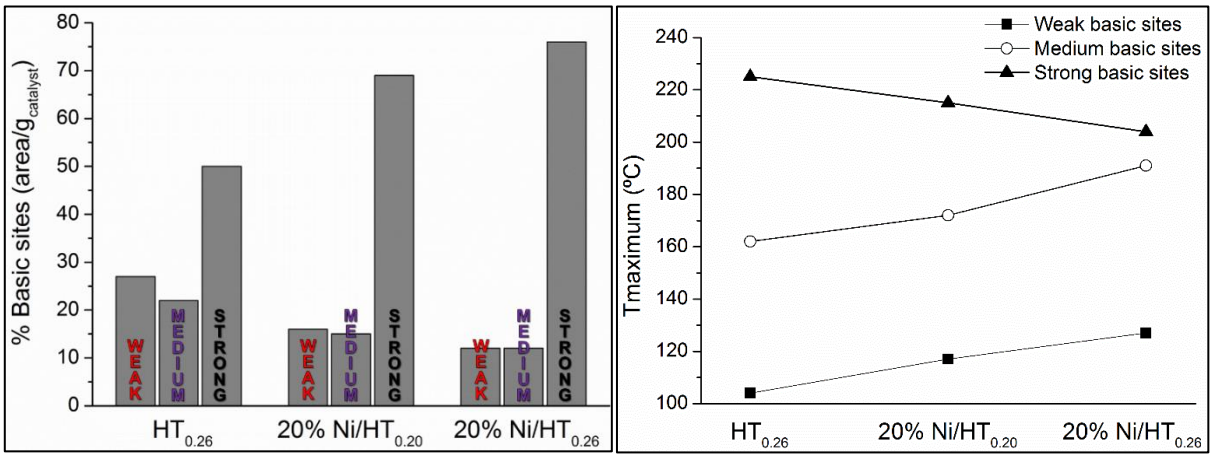

Figure 33: Comparison of different basic sites and maximum temperature for samples with different x ratios

4.2.2. Catalytic tests

The results obtained from the catalytic tests of the samples with different x values are presented in the Figure 34. Both in terms of conversion and selectivity, the results are quite similar for both samples. This could be attributed to the similar CO_2 adsorption capacities for the samples and the results already very close to the thermodynamic values. The close resemblance in the performance of these catalysts could also be due to experimental error.

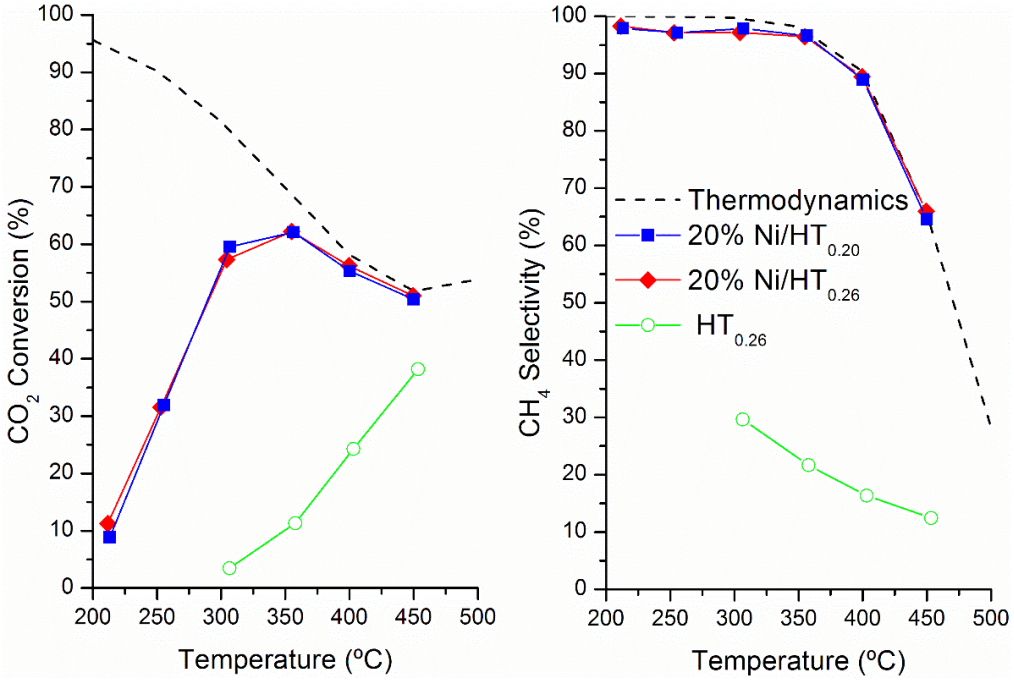

Figure 34: CO_2 conversion and CH_4 selectivity for samples with different x. Conditions: H_2:CO_2:Ar=4:1:95, GHSV=15000 $h^{-1}$and atmospheric pressure

4.2.3. Summary

The main results obtained in Section 4.2 are summarized in Table 12.

Table 12: Summary of results obtained in Section 4.2.

Technique	Main information inferred
FTIR	HT structure obtained irrespective of the x value
TG	Same profile was obtained irrespective of x. Two transitions were observed. The calcination temperature was determined (500ºC)
XRD	HT structure was verified in the non-calcined samples. NiO, $NiAl_2O_4$, MgO and solid solutions of NiO/MgO peaks were detected in the calcined samples
N_2 adsorption	The error of BET method is ca. +/- 5 %, so the registered differences are within experimental error; pore diameters and mesoporous volumes increases with x value
H_2-TPR	Lower x leads to the shift of the temperature of the main peak to lower value. The presence of NiO particles reduced at lower temperature
H_2-TPD	Higher x leads to lower dispersion and bigger average size for Ni^0 particles
CO_2-TPD	Three type of basic sites irrespective of Ni content
Catalytic tests	Similar results for the samples

4.3. Complementary studies

4.3.1. Effect of calcination and reduction

In order to evaluate the effects of the different thermal treatments in the sample properties, several characterization experiments were carried out with $HT_{0.26}$ and 20%Ni/$HT_{0.26}$ non-calcined, calcined and reduced samples.

Starting with **thermogravimetric studies**, the mass loss and heat flow profiles of $HT_{0.26}$ and 20% Ni/$HT_{0.26}$ are shown in Figure 35. As already reported in the present work, the profiles for non-calcined samples are the same even in presence of Ni, presenting two main transitions attributed to H_2O and carbonates decomposition. After calcination, the same type of profile is obtained for both samples. However, when compared with the non-calcined samples, different transitions can be observed. In both cases three processes can be observed at 100-150, 150-250 and 250-500ºC.

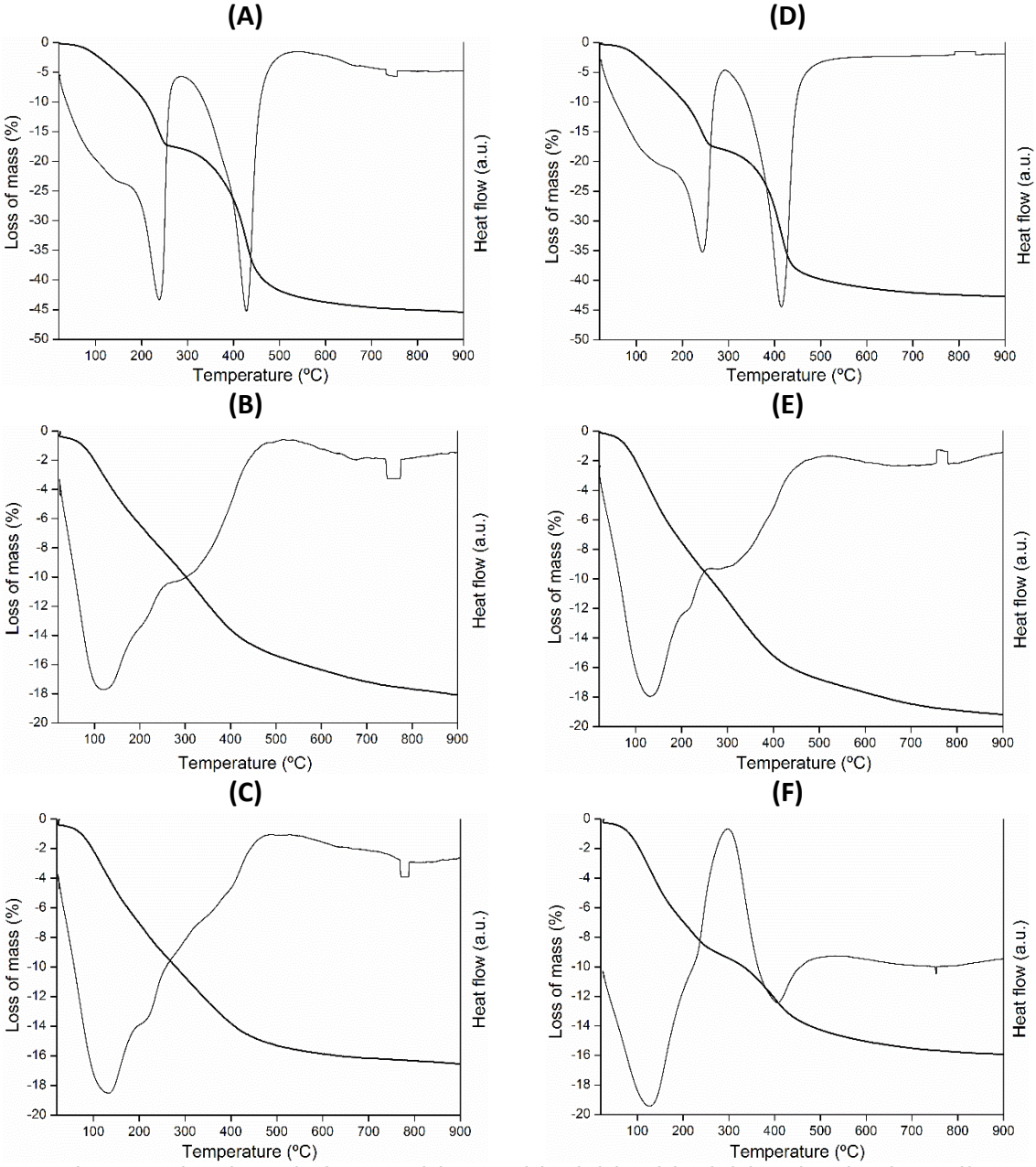

Figure 35. Thermogravimetric results for $HT_{0.26}$ (A) Non-calcined, (B) Calcined, (C) Reduced and 20%Ni/$HT_{0.26}$ (D) Non-calcined, (E) Calcined, (F) Reduced.

The **isotherms** obtained for both samples before calcination, after calcination and after reduction are shown in Figure 36. As it can be observed, the same type of isotherms was obtained irrespective of the heat treatment.

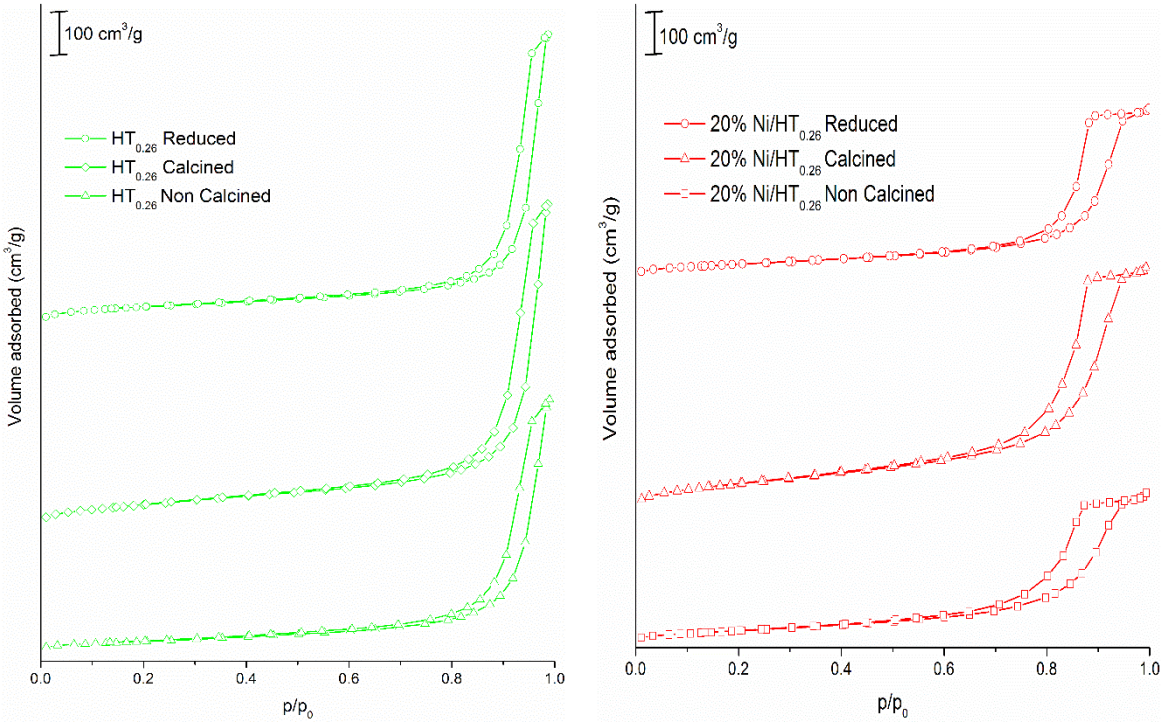

Figure 36: Isotherms obtained for samples non-calcined, calcined and reduced.

The **textural properties** obtained from the data analysis can be found in Table 13 and are compared in Figure 37.

Table 13: Textural properties determined for non-calcined, calcined and reduced samples.

Catalyst	S_{BET} (m^2/g)[a]	D_p (nm)[b]	V_{meso} (cm^3/g)[c]	V_{micro} (cm^3/g)[d]
$HT_{0.26}$ NC	106	45	0.697	0
$HT_{0.26}$	238	32	0.896	0.018
$HT_{0.26}$ Red	206	38	0.803	0.033
20% Ni/$HT_{0.26}$ NC	98	16	0.391	0
20% Ni/$HT_{0.26}$	236	16	0.654	0.011
20% Ni/$HT_{0.26}$ Red	93	16	0.445	0

[a] BET surface area;

[b] Pore diameter determined from the adsorption isotherms by BJH method;

[c,d] Pore volumes determined by t-plot method.

As it can be observed, calcination leads to an increase in the surface areas and the mesoporous volumes for both catalysts with and without Ni. However, reduction leads again to a decrease in these properties. In terms of pore diameters, calcination and reduction do not lead to changes in the Ni sample whereas for the $HT_{0.26}$ sample this characteristic decreases with calcination and slightly increases after reduction.

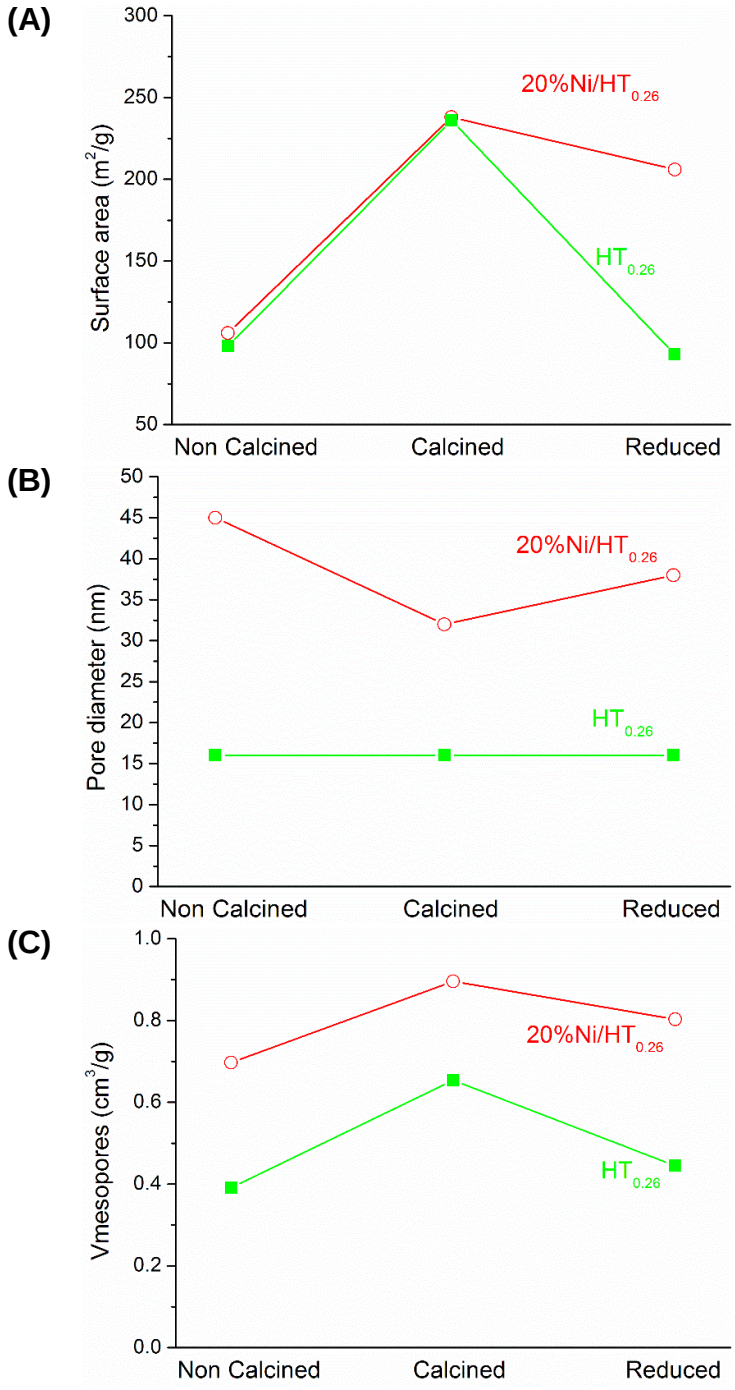

Figure 37: Comparison of textural properties for non-calcined, calcined and reduced samples of $HT_{0.26}$ and 20%Ni/$HT_{0.26}$.

The obtained **CO_2–TPD** profiles, similar for both samples are shown in Figure 38. For non-calcined samples a big peak of desorption above 300ºC, attributed to the decomposition of carbonate,

is present in the samples. After calcination the peak between 300-500ºC dramatically decreases due to the removal of most of the carbonates during the thermal treatment. After reduction the profiles do not present desorption of CO_2 above 300ºC. The other features of the profiles were already discussed in Sections 4.1.1 and 4.2.1.

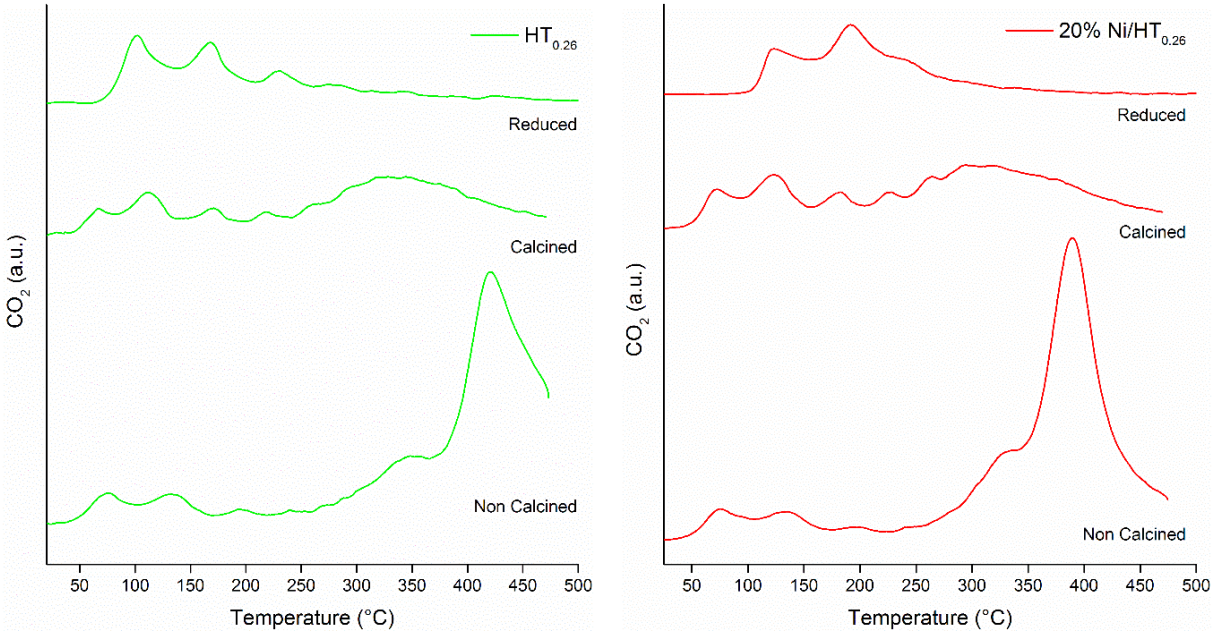

Figure 38: CO_2-TPD profiles for non-calcined, calcined and reduced samples.

In order to evaluate the **effect of reduction temperature on catalytic activity**, a sample (20% Ni/$HT_{0.26}$) was reduced at a lower temperature of 450°C and studied for its catalytic performance. As it can be seen from the Figure 39, both CO_2 conversion and CH_4 selectivity was much lower than when reduced at 800 °C. This is due the fact that only a small amount of Ni species was reduced at 450 °C according to H_2-TPR profile of this sample (Figure 21).

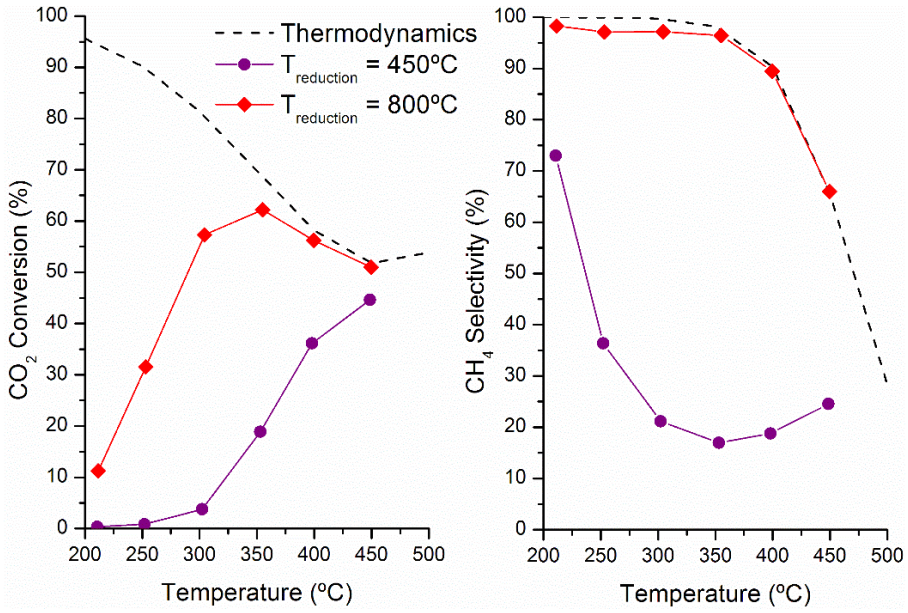

Figure 39: Comparison of the catalytic performance of 20% Ni/$HT_{0.26}$ reduced at 450 ºC and 800 ºC. Conditions: H_2:CO_2:Ar=4:1:95, GHSV=15000 h^{-1} and atmospheric pressure

4.3.2. Evaluation of the stability under reaction conditions: Long term test

A catalytic test of 24h at a reaction temperature of around 350ºC was carried out in order to evaluate the stability of one of the samples under study with time. The 20 Ni%/$HT_{0.26}$ sample was chosen because of being the one leading to better performances in the catalytic test. The results are shown in the Figure 40 and, as observed, the CO_2 conversion remained at around 57% and CH_4 selectivity at around 95% all throughout the test without any obvious decline of activity. The results are similar to those found in the literature [101]. This good stability of Ni–hydrotalcite derived catalysts provides a potential for its usage in industrial applications.

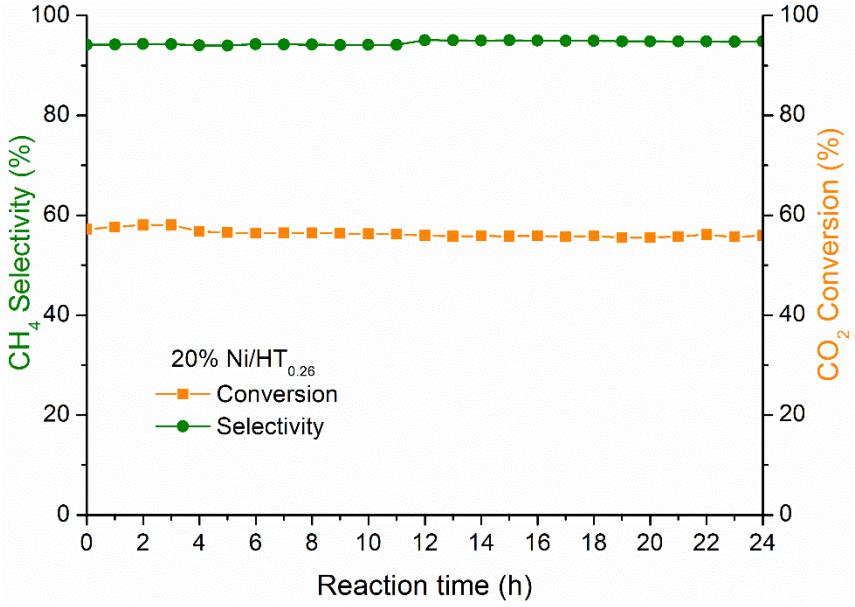

Figure 40: Long-term test results for catalyst 20%Ni/$HT_{0.26}$. Conditions: H_2:CO_2:Ar=4:1:95, GHSV=15000 h^{-1}, 350°C and atmospheric pressure

4.3.3. Comparison with commercial catalyst

In order to compare the catalytic results obtained by the Ni – hydrotalcite derived materials from the present study with commercially available catalyst, a commercial Ni/Al_2O_3 with 25 wt% Ni was tested under the same conditions.

As it can be seen, Figure 41 shows the comparison of commercial catalyst and 20% Ni/$HT_{0.26}$. From the figure it may be derived that the Ni based catalyst of the present study has better catalytic performances than the commercial one, even if the later presents more Ni particles reduced at lower temperature. As there are differences in the basicity of both catalysts, the enhanced CO_2 adsorption capacity of the hydrotalcite derived catalyst could be responsible for the better catalytic performance of this type of material.

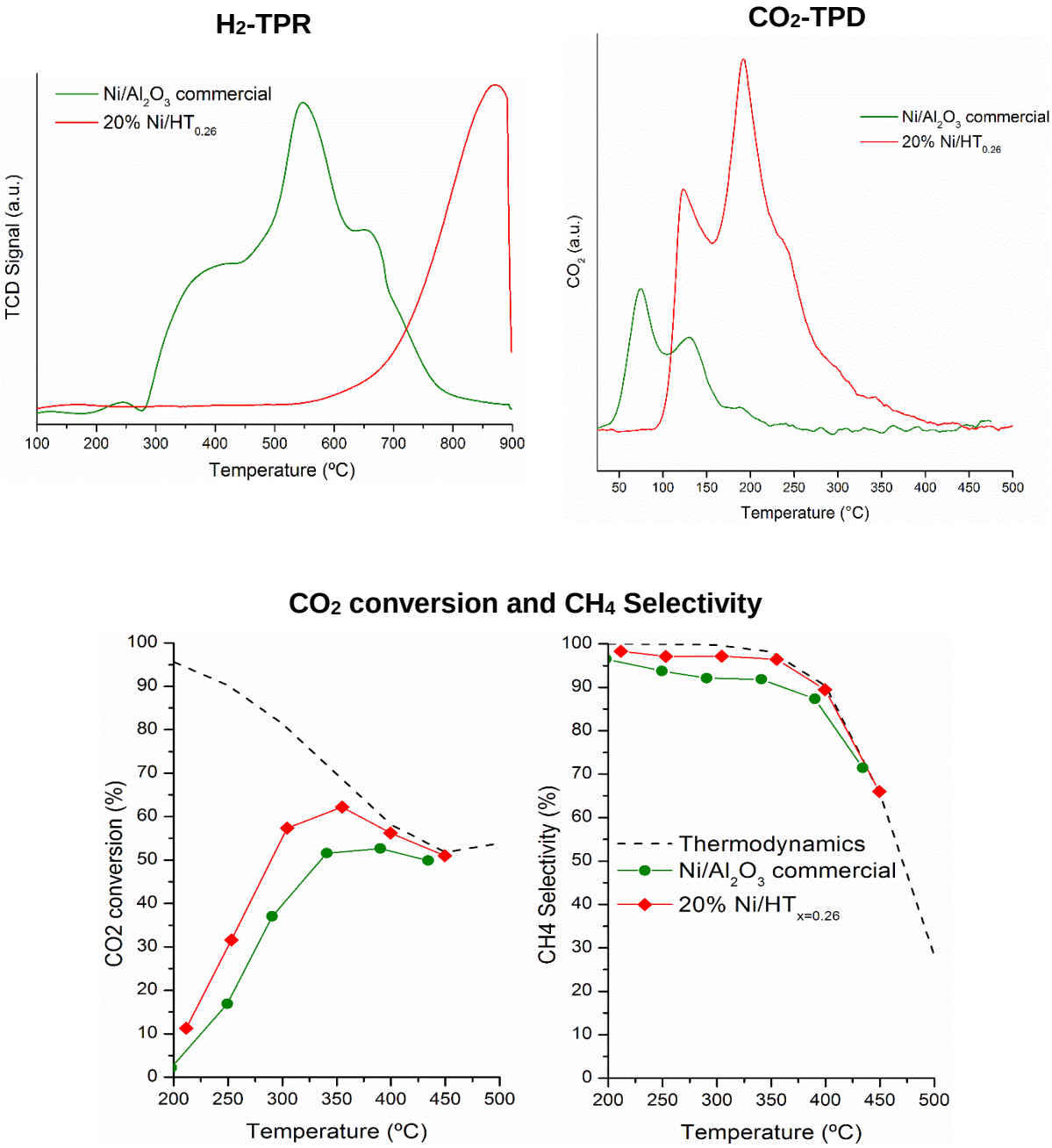

Figure 41: The comparison of commercial catalyst and 20%Ni/HT$_{0.26}$.

5. Conclusions

In the present work CO_2 methanation was studied using Ni-hydrotalcite derived catalysts. The effect of Ni content as well as x=M(III)/(M(III)+M(II)) ratios in different characterization techniques and catalytic performance were studied. All catalysts were synthesized by co-precipitation method and the structure was verified by FTIR and XRD characterization techniques as being that of typical hydrotalcite, irrespective of sample composition.

After the calcination of the materials at a temperature of 500°C which is established according to TGA results, hydrotalcite structure was removed. Thus, mixed oxides containing species such as NiO, MgO, $NiAl_2O_4$ or NiO/MgO solid solution irrespective of sample composition were formed as verified by XRD. The calcined materials were characterized by high specific surface areas in the range of 220-240 m^2/g. Pore diameters, as well as mesoporous volumes, were affected by Ni content and x (x=Al/Al+Mg+Ni) factor. On one hand, the increasing amounts of Ni led to lower diameters and volumes. On the other hand, the sample with x=0.26 has slightly bigger diameter and volume compared to the sample with x=0.20, due to the higher amount of carbonate species present in the sample with x=0.26 before calcination. In terms of dispersion, no significant trend was observed between samples with different Ni content whereas the dispersion increases for the sample with lower x. Regarding Ni^0 particle size, higher Ni content as well as higher x leads to bigger average Ni^0 particle size; and the values obtained (in the range of 50 nm) were much higher than those reported in the literature. In addition, all materials showed a high CO_2 adsorption capacity below 300ºC. The percentage of strong basic sites increased both with increase in the Ni content and x value.

In terms of catalytic performances, no important differences between catalysts were detected. However, higher Ni content led to a slight increase in CO_2 conversion and CH_4 selectivity. The prepared Ni–hydrotalcite derived catalyst was compared with a similar Ni content commercial catalyst. According to the results, Ni–hydrotalcite derived catalyst showed better performance both in CO_2 conversion CH_4 selectivity than the commercial catalyst.

A catalyst of the present study was active during 24h stability test at a reaction temperature of 350°C without any significant loss of catalytic performance; the CO_2 conversion remained at around 57% and CH_4 selectivity at around 95% all throughout the test without any obvious decline of activity.

Study of catalytic tests with different conditions (such as high GHSV, pressure, etc.,), optimization of Ni content, characterization of spent catalysts and samples reduced at 450 °C could be done in the future for the better understanding of this catalytic system in the hydrogenation of CO_2.

6. References

[1] US EPA CCD. Carbon Dioxide Emissions n.d. https://www3.epa.gov/climatechange/ghgemissions/gases/co2.html (accessed July 4, 2016).

[2] Earth's CO2 Home Page. CO2Earth n.d. https://www.co2.earth/ (accessed August 31, 2016).

[3] Ciais P, Sabine C, Bala G, Bopp L, Brovkin V, Canadell J, et al. Carbon and other biogeochemical cycles. Clim. Change 2013 Phys. Sci. Basis Contrib. Work. Group Fifth Assess. Rep. Intergov. Panel Clim. Change, Cambridge University Press; 2014, p. 465–570.

[4] Intergovernmental Panel on Climate Change, Edenhofer O, editors. Climate change 2014: mitigation of climate change: Working Group III contribution to the Fifth Assessment Report of the Intergovernmental Panel on Climate Change. New York, NY: Cambridge University Press; 2014.

[5] CO2 Emissions From Fuel Combustion Highlights 2015 n.d.

[6] CO2 Emissions From Fuel Combustions Highlights 2015.

[7] Energy and Climate Change 2015 - World Energy Outlook Special report 2015.

[8] Wang W, Wang S, Ma X, Gong J. Recent advances in catalytic hydrogenation of carbon dioxide. Chem Soc Rev 2011;40:3703..

[9] Yang H, Xu Z, Fan M, Gupta R, Slimane RB, Bland AE, et al. Progress in carbon dioxide separation and capture: A review. J Environ Sci 2008;20:14–27.

[10] York DG, Adelman J, Anderson Jr JE, Anderson SF, Annis J, Bahcall NA, et al. The sloan digital sky survey: Technical summary. Astron J 2000;120:1579.

[11] Aldous R. Carbon capture and storage – a vital part of our climate change response. The Conversation n.d. http://theconversation.com/carbon-capture-and-storage-a-vital-part-of-our-climate-change-response-3972 (accessed August 31, 2016).

[12] Graham-Rowe D. Lets hear it for CO2. New Sci 2008;197:32–4.

[13] Centi G, Perathoner S. Opportunities and prospects in the chemical recycling of carbon dioxide to fuels. Catal Today 2009;148:191–205.

[14] Sakakura T, Choi J-C, Yasuda H. Transformation of Carbon Dioxide. Chem Rev 2007;107:2365–87.

[15] Song C. Global challenges and strategies for control, conversion and utilization of CO2 for sustainable development involving energy, catalysis, adsorption and chemical processing. Catal Today 2006;115:2–32.

[16] Aresta M, Dibenedetto A. Utilisation of CO2 as a chemical feedstock: opportunities and challenges. Dalton Trans 2007:2975–92.

[17] Lunde PJ, Kester FL. Carbon Dioxide Methanation on a Ruthenium Catalyst. Ind Eng Chem Process Des Dev 1974;13:27–33.

[18] Park J-N, McFarland EW. A highly dispersed Pd–Mg/SiO2 catalyst active for methanation of CO2. J Catal 2009;266:92–7.

[19] Su X, Xu J, Liang B, Duan H, Hou B, Huang Y. Catalytic carbon dioxide hydrogenation to methane: A review of recent studies. J Energy Chem n.d.

[20] Medina JC, Butala SJ, Bartholomew CH, Lee ML. Iron-catalyzed CO2 hydrogenation as a mechanism for coalbed gas formation. Fuel 2000;79:89–93.

[21] Lapidus AL, Gaidai NA, Nekrasov NV, Tishkova LA, Agafonov YA, Myshenkova TN. The mechanism of carbon dioxide hydrogenation on copper and nickel catalysts. Pet Chem 2007;47:75–82.

[22] Shen W-J, Ichihashi Y, Ando H, Matsumura Y, Okumura M, Haruta M. Effect of reduction temperature on structural properties and CO/CO2 hydrogenation characteristics of a Pd-CeO2 catalyst. Appl Catal Gen 2001;217:231–9.

[23] Chang F-W, Kuo M-S, Tsay M-T, Hsieh M-C. Hydrogenation of CO2 over nickel catalysts on rice husk ash-alumina prepared by incipient wetness impregnation. Appl Catal Gen 2003;247:309–20.

[24] Yamasaki M, Habazaki H, Asami K, Izumiya K, Hashimoto K. Effect of tetragonal ZrO2 on the catalytic activity of Ni/ZrO2 catalyst prepared from amorphous Ni–Zr alloys. Catal Commun 2006;7:24–8.

[25] Du G, Lim S, Yang Y, Wang C, Pfefferle L, Haller GL. Methanation of carbon dioxide on Ni-incorporated MCM-41 catalysts: The influence of catalyst pretreatment and study of steady-state reaction. J Catal 2007;249:370–9.

[26] Brooks KP, Hu J, Zhu H, Kee RJ. Methanation of carbon dioxide by hydrogen reduction using the Sabatier process in microchannel reactors. Chem Eng Sci 2007;62:1161–70.

[27] Ocampo F, Louis B, Roger A-C. Methanation of carbon dioxide over nickel-based Ce0.72Zr0.28O2 mixed oxide catalysts prepared by sol–gel method. Appl Catal Gen 2009;369:90–6.

[28] GAO J, JIA L, FANG W, LI Q, SONG H. Methanation of carbon dioxide over the LaNiO3 perovskite catalysts activated under the reactant stream. J Fuel Chem Technol 2009;37:573–7.

[29] SONG H, YANG J, ZHAO J, CHOU L. Methanation of Carbon Dioxide over a Highly Dispersed Ni/La2O3 Catalyst. Chin J Catal 2010;31:21–3.

[30] Jiménez V, Sánchez P, Panagiotopoulou P, Valverde JL, Romero A. Methanation of CO, CO2 and selective methanation of CO, in mixtures of CO and CO2, over ruthenium carbon nanofibers catalysts. Appl Catal Gen 2010;390:35–44.

[31] Bakar WAWA, Ali R, Toemen S. Catalytic methanation reaction over supported nickel-rhodium oxide for purification of simulated natural gas. J Nat Gas Chem 2011;20:585–94.

[32] Sharma S, Hu Z, Zhang P, McFarland EW, Metiu H. CO2 methanation on Ru-doped ceria. J Catal 2011;278:297–309.

[33] Ocampo F, Louis B, Kiwi-Minsker L, Roger A-C. Effect of Ce/Zr composition and noble metal promotion on nickel based CexZr1−xO2 catalysts for carbon dioxide methanation. Appl Catal Gen 2011;392:36–44.

[34] Cai M, Wen J, Chu W, Cheng X, Li Z. Methanation of carbon dioxide on Ni/ZrO2-Al2O3 catalysts: Effects of ZrO2 promoter and preparation method of novel ZrO2-Al2O3 carrier. J Nat Gas Chem 2011;20:318–24.

[35] Zhi G, Guo X, Wang Y, Jin G, Guo X. Effect of La2O3 modification on the catalytic performance of Ni/SiC for methanation of carbon dioxide. Catal Commun 2011;16:56–9.

[36] Liu H, Zou X, Wang X, Lu X, Ding W. Effect of CeO2 addition on Ni/Al2O3 catalysts for methanation of carbon dioxide with hydrogen. J Nat Gas Chem 2012;21:703–7.

[37] da Silva DCD, Letichevsky S, Borges LEP, Appel LG. The Ni/ZrO2 catalyst and the methanation of CO and CO2. Int J Hydrog Energy 2012;37:8923–8.

[38] Beuls A, Swalus C, Jacquemin M, Heyen G, Karelovic A, Ruiz P. Methanation of CO2: Further insight into the mechanism over Rh/γ-Al2O3 catalyst. Appl Catal B Environ 2012;113–114:2–10.

[39] Hwang S, Hong UG, Lee J, Seo JG, Baik JH, Koh DJ, et al. Methanation of carbon dioxide over mesoporous Ni–Fe–Al2O3 catalysts prepared by a coprecipitation method: Effect of precipitation agent. J Ind Eng Chem 2013;19:2016–21.

[40] Abelló S, Berrueco C, Montané D. High-loaded nickel–alumina catalyst for direct CO2 hydrogenation into synthetic natural gas (SNG). Fuel 2013;113:598–609.

[41] Zhou G, Wu T, Xie H, Zheng X. Effects of structure on the carbon dioxide methanation performance of Co-based catalysts. Int J Hydrog Energy 2013;38:10012–8.

[42] Hwang S, Lee J, Hong UG, Baik JH, Koh DJ, Lim H, et al. Methanation of carbon dioxide over mesoporous Ni–Fe–Ru–Al2O3 xerogel catalysts: Effect of ruthenium content. J Ind Eng Chem 2013;19:698–703.

[43] Graça I, González LV, Bacariza MC, Fernandes A, Henriques C, Lopes JM, et al. CO2 hydrogenation into CH4 on NiHNaUSY zeolites. Appl Catal B Environ 2014;147:101–10.

[44] Rahmani S, Rezaei M, Meshkani F. Preparation of highly active nickel catalysts supported on mesoporous nanocrystalline γ-Al2O3 for CO2 methanation. J Ind Eng Chem 2014;20:1346–52.

[45] Aziz MAA, Jalil AA, Triwahyono S, Sidik SM. Methanation of carbon dioxide on metal-promoted mesostructured silica nanoparticles. Appl Catal Gen 2014;486:115–22.

[46] Guo M, Lu G. The effect of impregnation strategy on structural characters and CO2 methanation properties over MgO modified Ni/SiO2 catalysts. Catal Commun 2014;54:55–60.

[47] Toemen S, Bakar WAWA, Ali R. Investigation of Ru/Mn/Ce/Al2O3 catalyst for carbon dioxide methanation: Catalytic optimization, physicochemical studies and RSM. J Taiwan Inst Chem Eng 2014;45:2370–8.

[48] Garbarino G, Riani P, Magistri L, Busca G. A study of the methanation of carbon dioxide on Ni/Al2O3 catalysts at atmospheric pressure. Int J Hydrog Energy 2014;39:11557–65.

[49] Pan Q, Peng J, Sun T, Gao D, Wang S, Wang S. CO2 methanation on Ni/Ce0.5Zr0.5O2 catalysts for the production of synthetic natural gas. Fuel Process Technol 2014;123:166–71.

[50] Wan Abu Bakar WA, Ali R, Mohammad NS. The effect of noble metals on catalytic methanation reaction over supported Mn/Ni oxide based catalysts. Arab J Chem 2015;8:632–43.

[51] Garbarino G, Bellotti D, Riani P, Magistri L, Busca G. Methanation of carbon dioxide on Ru/Al2O3 and Ni/Al2O3 catalysts at atmospheric pressure: Catalysts activation, behaviour and stability. Int J Hydrog Energy 2015;40:9171–82.

[52] Fan Z, Sun K, Rui N, Zhao B, Liu C. Improved activity of Ni/MgAl2O4 for CO2 methanation by the plasma decomposition. J Energy Chem 2015;24:655–9.

[53] Ren J, Qin X, Yang J-Z, Qin Z-F, Guo H-L, Lin J-Y, et al. Methanation of carbon dioxide over Ni–M/ZrO2 (M = Fe, Co, Cu) catalysts: Effect of addition of a second metal. Fuel Process Technol 2015;137:204–11.

[54] Zhou G, Liu H, Cui K, Jia A, Hu G, Jiao Z, et al. Role of surface Ni and Ce species of Ni/CeO2 catalyst in CO2 methanation. Appl Surf Sci 2016;383:248–52.

[55] Ahmad W, Al-Matar A, Shawabkeh R, Rana A. An experimental and thermodynamic study for conversion of CO2 to CO and methane over Cu-K/Al2O3. J Environ Chem Eng 2016;4:2725–35.

[56] Toemen S, Wan Abu Bakar WA, Ali R. CO2/H2 methanation technology of strontia based catalyst: physicochemical and optimisation studies by Box–Behnken design. J Clean Prod n.d.

[57] García–García I, Izquierdo U, Barrio VL, Arias PL, Cambra JF. Power-to-Gas: Storing surplus electrical energy. Study of Al2O3 support modification. Int J Hydrog Energy n.d.

[58] Toemen S, Abu Bakar WAW, Ali R. Effect of ceria and strontia over Ru/Mn/Al2O3 catalyst: Catalytic methanation, physicochemical and mechanistic studies. J CO2 Util 2016;13:38–49.

[59] Koschany F, Schlereth D, Hinrichsen O. On the kinetics of the methanation of carbon dioxide on coprecipitated NiAl(O)x. Appl Catal B Environ 2016;181:504–16.

[60] Nizio M, Benrabbah R, Krzak M, Debek R, Motak M, Cavadias S, et al. Low temperature hybrid plasma-catalytic methanation over Ni-Ce-Zr hydrotalcite-derived catalysts. Catal Commun 2016;83:14–7.

[61] Garbarino G, Bellotti D, Finocchio E, Magistri L, Busca G. Methanation of carbon dioxide on Ru/Al2O3: Catalytic activity and infrared study. Catal Today n.d.

[62] Wierzbicki D, Debek R, Motak M, Grzybek T, Gálvez ME, Da Costa P. Novel Ni-La-hydrotalcite derived catalysts for CO2 methanation. Catal Commun 2016;83:5–8.

[63] Yan Y, Dai Y, He H, Yu Y, Yang Y. A novel W-doped Ni-Mg mixed oxide catalyst for CO2 methanation. Appl Catal B Environ 2016;196:108–16.

[64] Fujita S, Terunuma H, Kobayashi H, Takezawa N. Methanation of carbon monoxide and carbon dioxide over nickel catalyst under the transient state. React Kinet Catal Lett 1987;33:179–84.

[65] Sehested J, Dahl S, Jacobsen J, Rostrup-Nielsen JR. Methanation of CO over Nickel: Mechanism and Kinetics at High H2/CO Ratios. J Phys Chem B 2005;109:2432–8.

[66] Bacariza MC. From a greenhouse waste to a valuable raw material. Instituto Superior Tecnico, 2013.

[67] Aldana PAU, Ocampo F, Kobl K, Louis B, Thibault-Starzyk F, Daturi M, et al. Catalytic CO2 valorization into CH4 on Ni-based ceria-zirconia. Reaction mechanism by operando IR spectroscopy. Catal Today 2013;215:201–7.

[68] Westermann A, Azambre B, Bacariza MC, Graça I, Ribeiro MF, Lopes JM, et al. Insight into CO2 methanation mechanism over NiUSY zeolites: An operando IR study. Appl Catal B Environ 2015;174–175:120–5.

[69] Cavani F, Trifirò F, Vaccari A. Hydrotalcite-type anionic clays: Preparation, properties and applications. Catal Today 1991;11:173–301.

[70] Vaccari A. Preparation and catalytic properties of cationic and anionic clays. Catal Today 1998;41:53–71.

[71] Drits VA, Sokolova TN, Sokolova GV, Cherkashin VI. New members of the hydrotalcite-manasseite group. Clays Clay Miner 1987;35:401–417.
[72] Kannan S. Catalytic applications of hydrotalcite-like materials and their derived forms. Catal Surv Asia 2006;10:117–37.
[73] Mul G, Moulijn JA. Preparation of Supported Metal Catalysts. ChemInform 2005;36.
[74] Forano C, Costantino U, Prévot V, Gueho CT. Layered Double Hydroxides (LDH). Dev. Clay Sci., vol. 5, Elsevier; 2013, p. 745–82.
[75] Miyata S. Anion-exchange properties of hydrotalcite-like compounds. Clays Clay Min 1983;31:305–311.
[76] da Silva LFS, Demets GJ-F, Taviot-Guého C, Leroux F, Valim JB. Unusual Incorporation of Neutral and Low Water-Soluble Guest Molecules into Layered Double Hydroxides: The Case of Cucurbit[6 and 7]uril Inclusion Hosts. Chem Mater 2011;23:1350–2.
[77] Brindley GW, Kikkawa S. Thermal behavior of hydrotalcite and of anion-exchanged forms of hydrotalcite. Clays Clay Miner 1980;28:87–91.
[78] Mascolo G, Marino O. A new synthesis and characterization of magnesium-aluminium hydroxides. Miner Mag 1980;43:619–21.
[79] He J, Wei M, Li B, Kang Y, Evans DG, Duan X. Preparation of Layered Double Hydroxides. In: Duan X, Evans DG, editors. Layer. Double Hydroxides, Springer Berlin Heidelberg; 2006, p. 89–119.
[80] Gusi S, Trifirò F, Vaccari A, Del Piero G. Catalysts for low-temperature methanol synthesis. J Catal 1985;94:120–7.
[81] Costantino U, Marmottini F, Nocchetti M, Vivani R. New Synthetic Routes to Hydrotalcite-Like Compounds − Characterisation and Properties of the Obtained Materials. Eur J Inorg Chem 1998;1998:1439–46.
[82] Rajamathi M, Kamath PV. Urea hydrolysis of cobalt(II) nitrate melts: synthesis of novel hydroxides and hydroxynitrates. Int J Inorg Mater 2001;3:901–6.
[83] Reichle WT. Synthesis of anionic clay minerals (mixed metal hydroxides, hydrotalcite). Solid State Ion 1986;22:135–41.
[84] Marchi AJ, Apesteguía CR. Impregnation-induced memory effect of thermally activated layered double hydroxides. Appl Clay Sci 1998;13:35–48.
[85] Miyata S. Hydrotalcites in relation to composition. Clays Clay Min 1980;28:50–56.
[86] Mekyoung Kim. Predicting thermally thin burning of polymer using TGA/DSC. University of Maryland, 2006.
[87] Leofanti G, Padovan M, Tozzola G, Venturelli B. Surface area and pore texture of catalysts. Catal Today 1998;41:207–19.
[88] Fadoni M, Lucarelli L. Temperature programmed desorption, reduction, oxidation and flow chemisorption for the characterisation of heterogeneous catalysts. Theoretical aspects, instrumentation and applications. Stud. Surf. Sci. Catal., vol. 120, Elsevier; 1999, p. 177–225.
[89] Joy DC. The theory and practice of high-resolution scanning electron microscopy. Ultramicroscopy 1991;37:216–33.

[90] Pavel OD, Tichit D, Marcu I-C. Acido-basic and catalytic properties of transition-metal containing Mg–Al hydrotalcites and their corresponding mixed oxides. Appl Clay Sci 2012;61:52–8.

[91] Perez-Lopez OW, Senger A, Marcilio NR, Lansarin MA. Effect of composition and thermal pretreatment on properties of Ni–Mg–Al catalysts for CO2 reforming of methane. Appl Catal Gen 2006;303:234–44.

[92] Tichit D, Medina F, Coq B, Dutartre R. Activation under oxidizing and reducing atmospheres of Ni-containing layered double hydroxides. Appl Catal Gen 1997;159:241–58.

[93] Hu D, Gao J, Ping Y, Jia L, Gunawan P, Zhong Z, et al. Enhanced Investigation of CO Methanation over Ni/Al $_2$ O $_3$ Catalysts for Synthetic Natural Gas Production. Ind Eng Chem Res 2012;51:4875–86.

[94] Guo J, Lou H, Zhao H, Zheng X. Improvement of stability of out-layer MgAl2O4 spinel for a Ni/MgAl2O4/Al2O3 catalyst in dry reforming of methane. React Kinet Catal Lett 2005;84:93–100.

[95] Zhang J, Zhao N, Wei W, Sun Y. Partial oxidation of methane over Ni/Mg/Al/La mixed oxides prepared from layered double hydrotalcites. Int J Hydrog Energy 2010;35:11776–86.

[96] Lin X, Li R, Lu M, Chen C, Li D, Zhan Y, et al. Carbon dioxide reforming of methane over Ni catalysts prepared from Ni–Mg–Al layered double hydroxides: Influence of Ni loadings. Fuel 2015;162:271–80.

[97] Prinetto F, Ghiotti G, Graffin P, Tichit D. Synthesis and characterization of sol–gel Mg/Al and Ni/Al layered double hydroxides and comparison with co-precipitated samples. Microporous Mesoporous Mater 2000;39:229–47.

[98] Di Cosimo JI, Dıez VK, Xu M, Iglesia E, Apesteguıa CR. Structure and surface and catalytic properties of Mg-Al basic oxides. J Catal 1998;178:499–510.

[99] Corma A, Fornés V, Martín-Aranda RM, Rey F. Determination of base properties of hydrotalcites: Condensation of benzaldehyde with ethyl acetoacetate. J Catal 1992;134:58–65.

[100] Wiyantoko B, Kurniawati P, Purbaningtias TE, Fatimah I. Synthesis and Characterization of Hydrotalcite at Different Mg/Al Molar Ratios. Procedia Chem 2015;17:21–6.

[101] Abate S, Barbera K, Giglio E, Deorsola F, Bensaid S, Perathoner S, et al. Synthesis, Characterization, and Activity Pattern of Ni–Al Hydrotalcite Catalysts in CO2 Methanation. Ind Eng Chem Res 2016;55:8299–308.